Fall 2009

Stressed-eye analysis and jitter separation for high-speed serial links

Nitin Radhakrishnan

Department:

STRESSED-EYE ANALYSIS AND JITTER SEPARATION FOR HIGH-SPEED SERIAL LINKS

by

NITIN RADHAKRISHNAN

A THESIS

Presented to the Faculty of the Graduate School of the

MISSOURI UNIVERSITY OF SCIENCE AND TECHNOLOGY

In Partial Fulfillment of the Requirements for the Degree

MASTER OF SCIENCE IN COMPUTER ENGINEERING

2009

Approved by

Dr. Jun Fan, Advisor
Dr. James L. Drewniak
Dr. David J. Pommerenke

ABSTRACT

As the computer and electronics industry moves towards higher data rates, the most important concern in the field of signal integrity is jitter. A data communication link path often consists of a transmitter, a channel, and a receiver. Many mechanisms can contribute to jitter, a timing uncertainty in the received signal. For example, transmitters have intrinsic noise sources that contribute to random jitter and to certain types of deterministic jitter. In addition, external coupling may cause periodic jitter. The bandwidth limitation of the channel also contributes to a fourth type of jitter, inter-symbol interference. This thesis studies the various components of jitter and uses mathematical models of them to simulate an actual transmitter. These models allow the injection of various jitter components for stressed-eye testing.

To understand the sources of jitter in a received signal, this work studies the manifestation of each jitter component in the time-interval error spectrum is studied and develops procedures to separate the jitter components. These jitter decomposition procedures are compared and validated with real-time and sampling scopes. Bathtub curves and jitter transfer functions were also calculated to facilitate high-speed link path designs.

Based on the link-path and jitter analysis algorithms developed here, a cable certification tool was also designed to certify the small form factor pluggable copper cable assemblies against SFF-8431 specifications. This project implemented the framework of the certification tool.

ACKNOWLEDGMENTS

I would like to express my utmost gratitude to my advisor, Dr. Jun Fan, for his constant support and guidance throughout the course of my master's degree program.

I wish also to extend a special thanks to my committee members, Dr. James L. Drewniak and Dr. David J. Pommerenke, for their valuable input on my work.

I also thank Brice Achkir and Abhilash Rajagopal at Cisco Systems for their valuable research, and technical input, and advice that helped me finish my thesis.

Special thanks go to all those in the EMC Laboratory for their assistance and moral support.

Finally, I thank my parents, sister, brother-in-law, and nephew for their constant emotional support and encouragement. I wish to dedicate this work to them.

TABLE OF CONTENTS

LIST OF ILLUSTRATIONS

LIST OF TABLES

1. INTRODUCTION

With the continuous development of technology, electronic circuits become smaller and operate at higher data rates. For example, the 10 Gigabit Ethernet specifies a data rate of 10.3125Gbps. One of the main challenges of maintaining reliable data communication is jitter. Jitter is the primary quantity that limits the integrity of a signal as it moves from one test point to another in a link path. The main challenge in the industry is to reduce the effects of jitter on the signal and thereby ensure a reasonably low bit error rate (BER) for a link path [1].

1.1. WHAT IS JITTER?

Jitter can be defined as deviation from the ideal timing of an event. The reference event is the differential zero crossing for electrical events and the nominal receiver threshold power level for optical systems [2]. These points are represented in Figure 1.1.

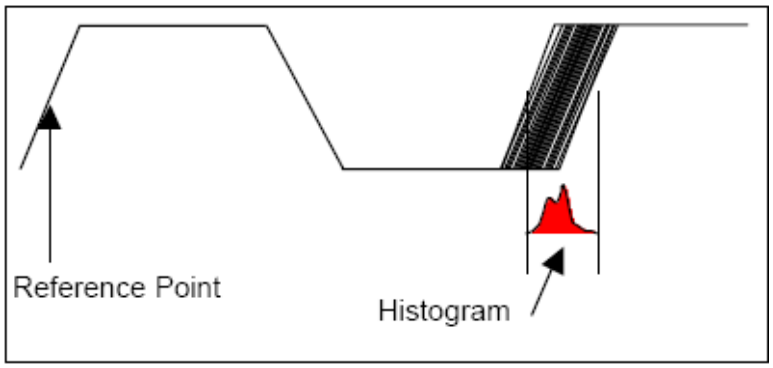

Figure 1.1. Jitter and histogram

An analysis in the frequency domain demonstrates the effect of channel losses on a signal. A signal in the frequency domain has spectral lines that contain two sets of information [3]. The low-frequency components define amplitude, and the high-

frequency components define the rise/fall time of the signal. Figure 1.2 shows a PRBS-9 signal operating at a data rate of 6.25Gbps. In the frequency domain this signal has spectral lines that repeat at the multiples of the data pattern, i.e., data rate divided by the number of bits per repetition is equal to 6.25Gbps divided by 511 which in turn is equal to 12.23MHz. Assuming a 31" long link path that transmits the signal, the differential transfer S-parameter of the trace can be considered as a low-pass filter that attenuates the high-frequency components more than the low-frequency ones.

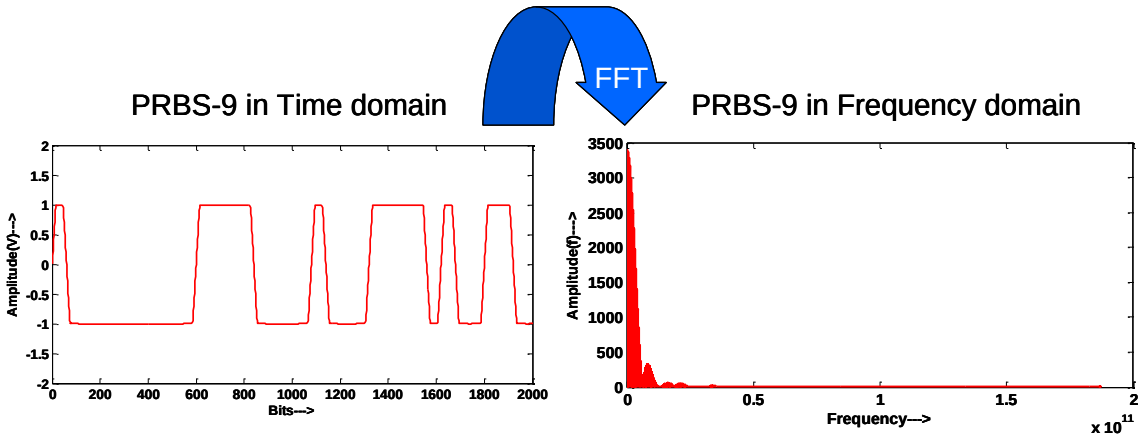

Figure 1.2. PRBS-9 signal in the time and frequency domain

A consequence of the filtering effect is that once the signal has finished its travel on the trace, its high-frequency components are attenuated more than those of the low-frequency components. Figure 1.3 illustrates this channel filtering effect.

As Figure 1.4 makes clear, when the output signal is reconstructed in the time domain (by taking inverse fourier transform), it has amplitude distortion and rise/fall time degradation due to the frequency-dependent loss of the channel.

Figure 1.4 compares the input signal and output signal. This effect of the channel on the signal is called inter-symbol interference (ISI). This effect limits a digital system by making the signal less digital, thus creating amplitude uncertainty, timing uncertainty, and a limited rise/fall time. ISI is one of the data-dependent jitter components that is

correlated to the data. Other forms of jitter become embedded in the signal before entering the channel, as explained in the section 1.2 below.

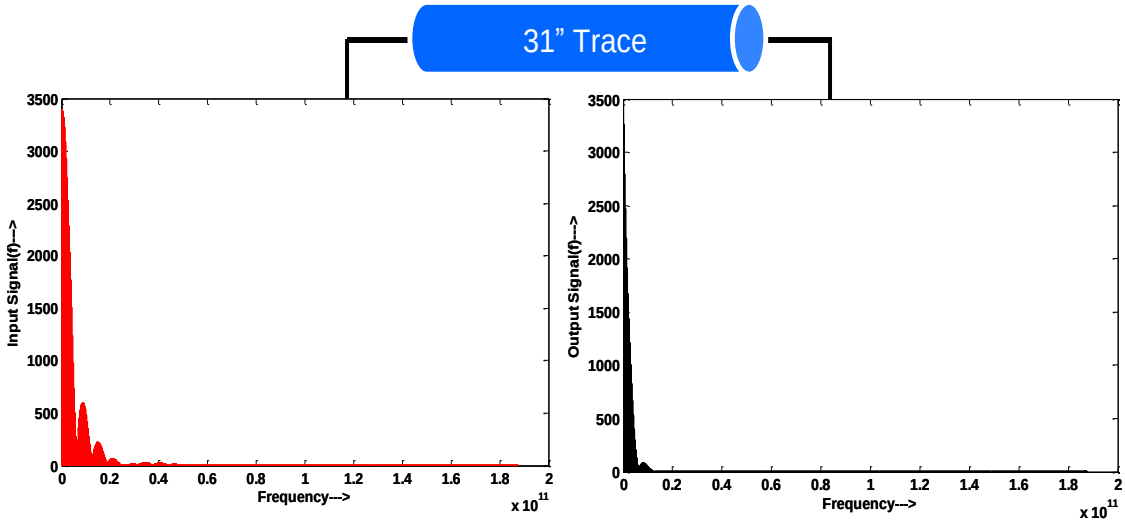

Figure 1.3. Channel filtering

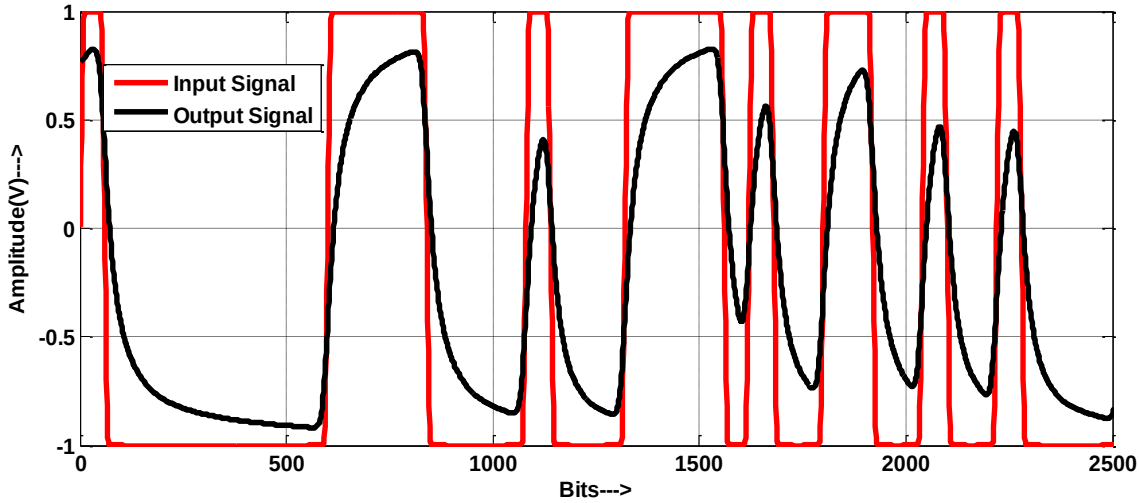

Figure 1.4. Input and output signal in time domain

1.2. JITTER INJECTION AND DECOMPOSITION

ISI is not the only form of jitter that can distort signal waveforms. Other deterministic and random components of jitter may be injected at the transmitter or during signal propagation in the channel. A transmitter always has some intrinsic jitter that acts as a source of random jitter (RJ). Noise coupling and crosstalk mechanisms cab result in periodic jitter (PJ). Incorrect voltage levels and zero crossings may introduce duty-cycle distortion (DCD) at the transmitter and be escalated under the influence of channel distortion.

Section 2 studies mathematical models of these types of jitter components and simulates an actual transmitter in the link path analyzer tool. To validate the jitter injection algorithms thus developed, eye diagrams and histograms are plotted and compared with available jitter models in Section 3.

In addition, various jitter components must be decomposed to determine the effect of each component on signal quality. Therefore, this work designed a jitter decomposition module and incorporated it into the link path analyzer tool. Such a model is possible because multiple TIE patterns are available for various jitter components. Section 4 describes the decomposition protocols developed based on a study of individual manifestations of the various jitter components in the TIE spectrum.

Section 5 discusses the decomposition algorithms that were developed based on a combination of spectral analysis and mathematical calculations. The jitter decomposition module has a well designed GUI with the ability to plot the TIE trend, histogram, and spectrum at three different test points. The transfer functions of the jitter components among the test points can be studied through the decomposed jitter values or by the use of bathtub curves.

Real-time scopes and sampling scopes from commercial vendors can perform jitter analysis and decomposition on the waveforms captured from a channel output. This work compared all the available instruments with the algorithms developed here. The results reveal that sampling scopes perform satisfactorily decompose RJ and PJ, but they are not good at analyzing DCD and ISI. On the other hand, real-time scopes effectively decompose DCD and ISI but show incorrect values for RJ and PJ.

1.3. CABLE CERTIFICATION TOOL

Small form factor pluggable (SFP+) modules are hot-pluggable serial-to-serial data agnostic optical transceivers [4]. They can be used in conjunction with optic fibers and copper cables. When copper cables are used, the transmission length is limited to 10m. The SFF-8431 specifications for enhanced SFP+ Module SFP+ modules include a set of parameters required to certify the SFP+ cable assemblies and their measurement procedures. This work studied five parameters discussed below in Section 6:

- dWDP (difference in dispersion penalty of output and input waveform)
- VMA (voltage modulation amplitude)
- DDPWS (pulse width shrinkage)
- Qsq (signal-to-noise ratio)
- RN (relative noise)

The standards are defined for a PRBS-9 pattern running at 10.3125Gbps. This work proposes a framework that can be used to develop and implement a complete cable certification tool. The tool can calculate the five parameters and write the results into a Word file through the use of a Matlab graphical user interface.

2. TYPES OF JITTER

Jitter components can be categorized based on two criteria: 1) whether they have a bounded or unbounded value and 2) whether they are correlated or uncorrelated to data. Figure 2.1 shows the various types of jitter components, based on these criteria.

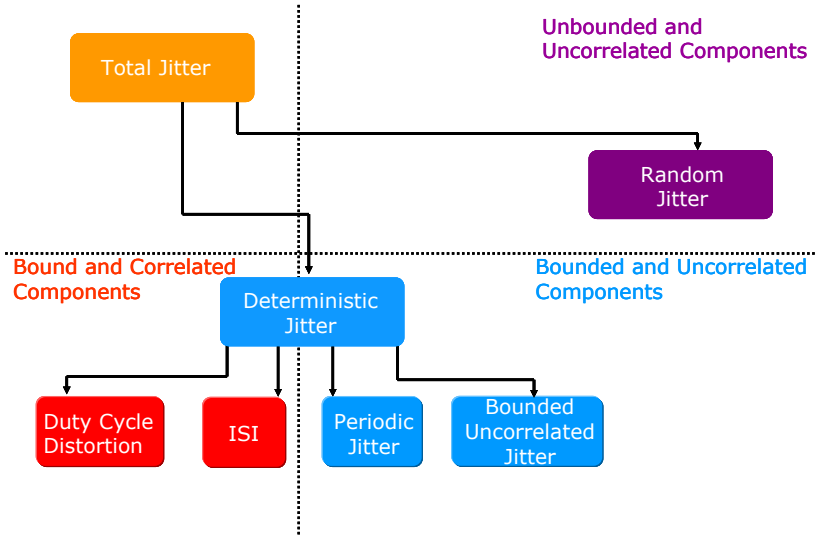

Figure 2.1. Jitter classification

Based on the first criterion, jitter can be divided into random jitter (RJ) and deterministic jitter (DJ). RJ is uncorrelated to data and does not have a bounded value. It can be specified in a root mean square (rms) value and has an approximate peak-to-peak value depending on the bit error rate (BER). DJ can be broken down further based on the second criterion; its components have a bounded value. Duty-cycle distortion (DCD) and inter-symbol interference (ISI) are correlated to data. Periodic jitter (PJ) and bounded uncorrelated jitter (BUJ) are usually uncorrelated to data.

2.1. RANDOM JITTER (RJ)

Random jitter is unbounded and uncorrelated. It is caused by unbounded jitter sources that have noise processes in the form of thermal noise, 1/f flicker noise, shot noise, and other high-order noise mechanisms. RJ causes random variation in the phase of the data stream. Since RJ is unbounded, it does not have a definite peak-to-peak value and is thus specified in RMS values. A reasonable approximation of the peak-to-peak value of RJ depends on the BER and is related to the RMS value of RJ by the following equation:

$$RJ_{pp} = \alpha * RJ_{rms} \tag{1}$$

where the value of α (scaling factor) is calculated from the BER. The mathematical model or histogram for RJ is given by a Gaussian bell distribution, as shown in Figure 2.2. The nominal range of RJ (rms) is approximately 0-1.5ps. RJ is usually not affected by the non ideal behaviors of the channel.

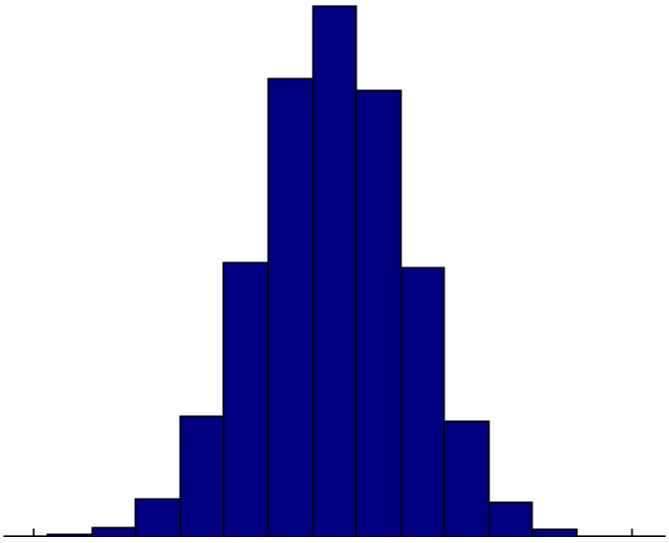

Figure 2.2. Histogram of RJ

2.2. PERIODIC JITTER (PJ)

Periodic Jitter is bounded but usually uncorrelated. It can be caused by external noise coupling and crosstalk, power supply noise, PLL comparator frequency feed-

through, etc. PJ can cause periodic variations in the phase of the data stream. It can be modeled as a sinusoidal jitter source modulated in phase with a data stream. The sinusoidal jitter source is defined as

$$A_{PJ} * \sin(2\pi f_{PJ} t) \tag{2}$$

where A_{PJ} is the peak-to-peak magnitude of PJ, which has an approximate nominal range of 0 to 4ps, and f_{PJ} is the frequency, which is usually less than 100 MHz. As shown in Figure 2.3, the largest probability distribution in the mathematical model or histogram of PJ is close to the peak values. As demonstrated in Section 4.1 this corresponds to the histogram of a sine wave. PJ is usually unaffected by the nonideal behaviors of the channel.

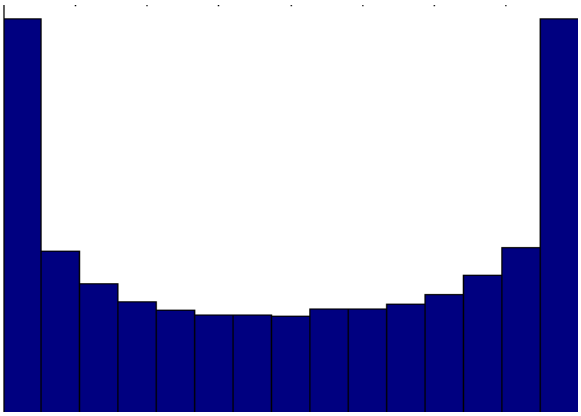

Figure 2.3. Histogram of PJ

2.3 DUTY-CYCLE DISTORTION (DCD)

Duty-cycle distortion falls under the category of bounded jitter correlated to data. It is caused by amplitude offsets, turn-on delays, and saturation effects. In the jitter analyzers typical in today's commercial context, an incorrect reference level during jitter analysis can lead to registration of a value of DCD in the readings. DCD affects performance in two ways: It first occurs at the output of the transmitter, for example due to the offset in the amplitude of the data stream. Further, DCD can be escalated by the

rise/fall time degradation caused by the channel losses. Thus, the total DCD seen at the input of the receiver (Rx) is the sum of the DCD at the transmitter (Tx) output and the DCD change caused by the channel. This is represented as

$$DCD_{input(Rx)} = DCD_{output(Tx)} + DCD_{channel}. \quad (3)$$

As shown in Figure 2.4, at peak values the mathematical model or histogram of DCD has a dual delta distribution. As demonstrated in Section 4.1 below, this corresponds to the histogram of a square wave.

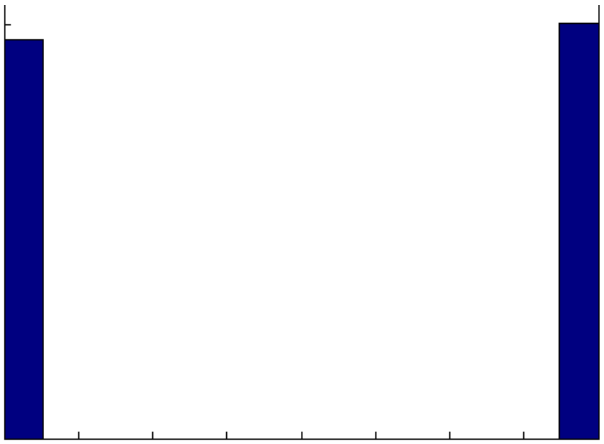

Figure 2.4. Histogram of DCD

2.4. INTER-SYMBOL INTERFERENCE (ISI)

Inter-symbol Interference is bounded jitter correlated to data. It occurs when the impulse response of the channel is longer than a data bit. As explained above, the bandwidth limitation of the channel attenuates the high-frequency components more than it does the low-frequency components. The direct consequence of this effect is that at the input of the receiver (Rx), the received waveforms are distorted with a reduced amplitude limitation and degraded rise/fall time. ISI does not have a mathematical model or histogram and is best modeled by a low-pass filter with a specified bandwidth, such as that shown in Figure 2.5.

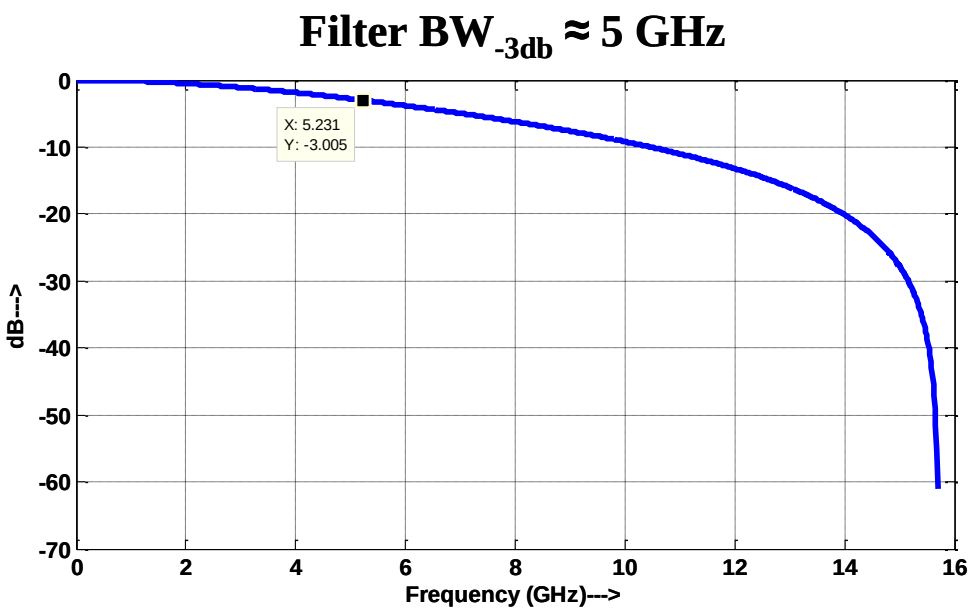

Figure 2.5. ISI modeled as a low-pass filter

3. STRESSED EYE ANALYSIS AND JITTER INJECTION

One of the important contributions of this research is to model a real-world transmitter through the use of eye diagrams. The eye diagram is simply the superposition over one unit interval of all the zero–to–one and one–to-zero transitions, each preceded and followed by various combinations of one and zero, and by constant levels of one and zero. Pattern generators usually have intrinsic noises (e.g., thermal noise or shot noise) that contribute to RJ in the pattern that is used as traffic. In addition, they may also be modulated by PJ sources such as external coupling into the circuit, power supply noise, PLL comparator, and frequency feed-through. DCD is also introduced into the pattern in the form of amplitude offset. In addition, it may also display some filtering effects in the form of cables before the pattern is actually launched into the channel. Figure 3.1 shows how a clean signal is distorted as it goes through a link path under the influence of the injection of various jitter components.

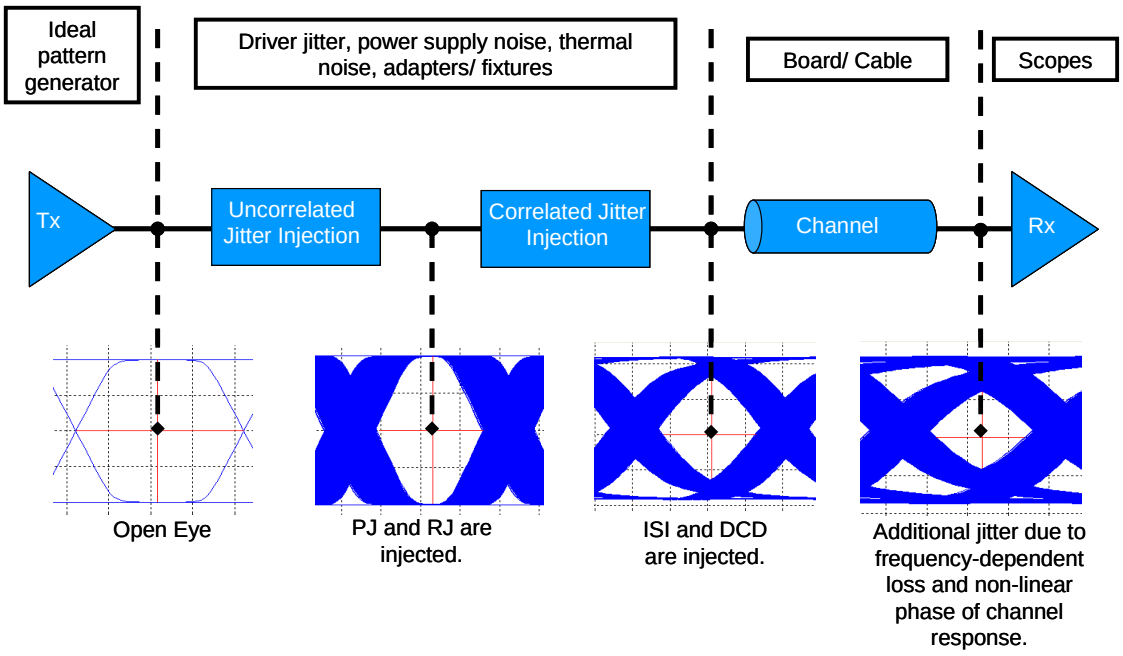

Figure 3.1. Stressed jitter analysis

To model this in the link path analyzer tool, this work uses various mathematical models available for jitter components. First, a protocol was selected for the order of components injections [5]. This protocol is represented in Figure 3.2. In the following sections, input to the channel is referred to as "Output of Tx," and output taken from the channel is referred to as "Input to Rx."

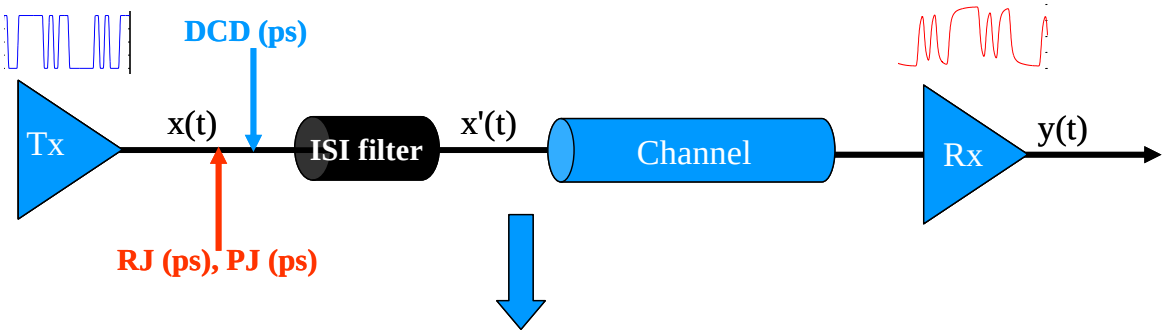

Figure 3.2. Jitter injection protocol

RJ and PJ are convoluted to form a dual-dirac distribution that is injected first by modulating the phase of signal x(t) at the output of Tx. A voltage offset corresponding to the amount of DCD required is then added. This offset is represented as V_{DCD}. At this point ISI filters representing an extra source of bandwidth limitation are added before the actual channel under consideration. They are defined by cut-off frequency, order, and gain. The final distorted waveform x'(t) passing into the channel can be summarized by the following equation:

$$x'(t) = ISI_{filter}(x[t + n(t)] + V_{DCD}) \tag{4}$$

where n(t) is equal to n'(t) convoluted with $A_{PJ} \sin(\omega_{PJ} t)$. This expression represents the convolution between RJ and PJ to yield a dual-dirac distribution that modulates the phase of x(t). The method of distortion is explained in detail in Section 3.1 and 3.2 below. Figure 3.3 shows the Matlab GUI depicting the jitter injection portion of the tool. The user has the option of providing the jitter values in the user-friendly GUI. The nominal range of each jitter component is also included. For random jitter, the value is specified

as an rms value. DCD is accepted as a peak-peak value. To add periodic jitter, the peak-peak value and frequency must be supplied. To add a cable effect to model ISI, a separate GUI with filter options is provided.

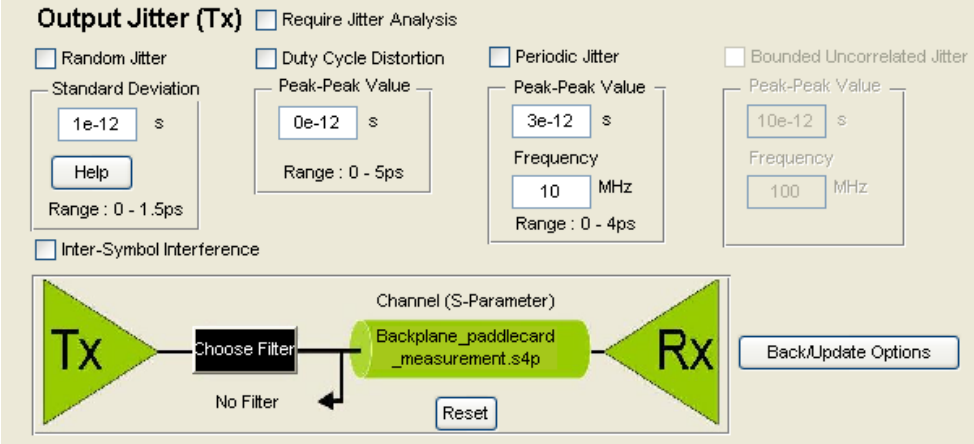

Figure 3.3. Matlab GUI for jitter injection

3.1. RJ INJECTION

To inject RJ, a set of random numbers n(t) is first generated with Gaussian distribution and a standard deviation selected by the user. This set is used to modulate the phase of the data stream used in transmission.

To cofirm that RJ has been injected properly, a clock sequence distorted with RJ of standard deviation 2ps is transmitted through a transmission line. The clock is used instead of PRBS because it is not affected by ISI. The eye diagram and the histogram at the input of Rx should record only the distortion caused by RJ. This simulation uses 3000 bits of clock. Assuming 1 error in 3000 bits, a BER of 1/3000 should correspond to a scaling factor of 7.1763. Based on equation (1) RJ_{pp} should amount to 14.35ps. Figure 3.4 shows the eye diagram and histogram screenshot from the link path analyzer tool. The histogram clearly shows a Gaussian distribution with a jitter peak-to-peak value of 14.7ps, which agrees with the calculated results.

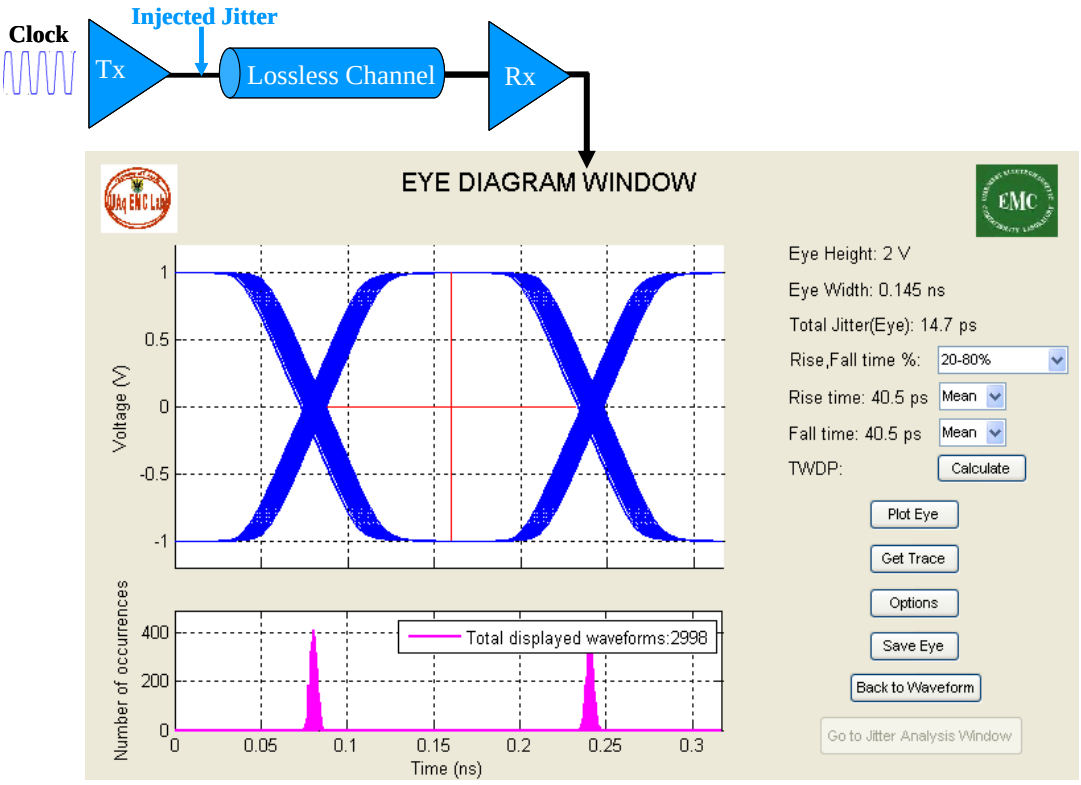

Figure 3.4. Eye diagram and histogram for injected jitter of RJ=2ps (rms)

3.2. PJ INJECTION

To inject PJ, a sinusoidal distribution A_{PJ} sin (ω_{PJ} t) is generated. As demonstrated, PJ is defined by the amplitude A_{PJ} and frequency f_{PJ}. Both these values can be fed into the tool. The distribution thus generated is then used to modulate the phase of data stream used in transmission. To determine whether the PJ has been injected properly, a clock sequence distorted with PJ of amplitude 50ps (exaggerated) and frequency 10 MHz is transmitted through a transmission line. PJ has an additive property when the total jitter at the input to Rx is analyzed. Since clock suffers no distortion in the channel caused by ISI, the jitter monitored at the input to Rx should be caused only by the injected PJ amplitude. Figure 3.5 shows the eye diagram and histogram screenshot from the link path analyzer tool. The histogram clearly shows a dual-dirac profile with some probability hits between the peak-to-peak values. The recorded value of jitter is 48ps, which if fairly close to the injected PJ value of 50ps.

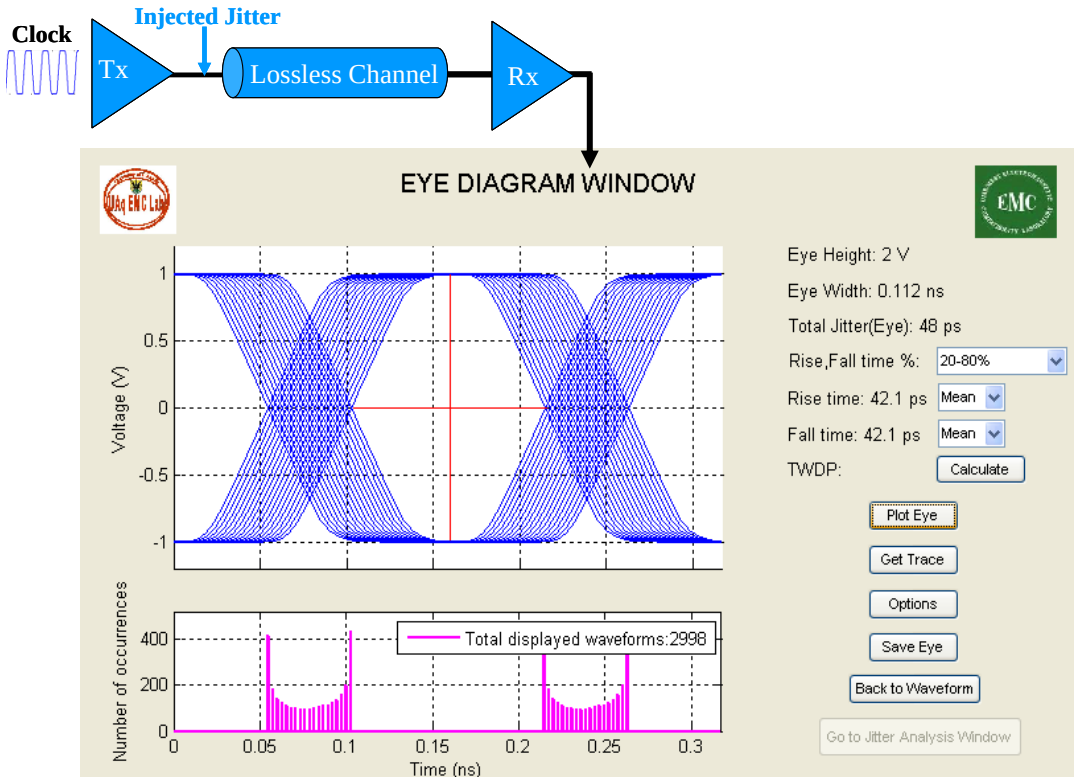

Figure 3.5. Eye diagram and histogram for injected jitter of PJ=50ps (peak-peak)

When both PJ and RJ are selected in the GUI, a sinusoidal distribution is individually generated corresponding to PJ, along with a random set of numbers of Gaussian distribution corresponding to RJ. These numbers are then convoluted to obtain an entity that has a histogram with dual-dirac distribution and Gaussian tails. The convolution can be represented as:

$$n(t) = n'(t) \otimes A_{PJ} \sin(w_{PJ} t) \tag{5}$$

where n(t) is then used to modulate the phase of data stream used in transmission. To determine whether the PJ has been injected properly, a clock sequence (3000 bits) distorted with PJ of amplitude 50ps (exaggerated) and frequency 10 MHz along with an RJ of 2ps (rms) is transmitted through a transmission line. Since the effect of ISI does not distort the clock in this case, the total jitter monitored at the input to Rx will be approximately 50ps plus (7.1758 multiplied with 2ps) which is approximately equal to 64ps. Figure 3.6 shows the eye diagram and histogram screenshot from the link path

analyzer tool. The histogram clearly shows a dual-dirac distribution with Gaussian tails. The jitter recorded is 62ps, which is fairly close to the calculated value.

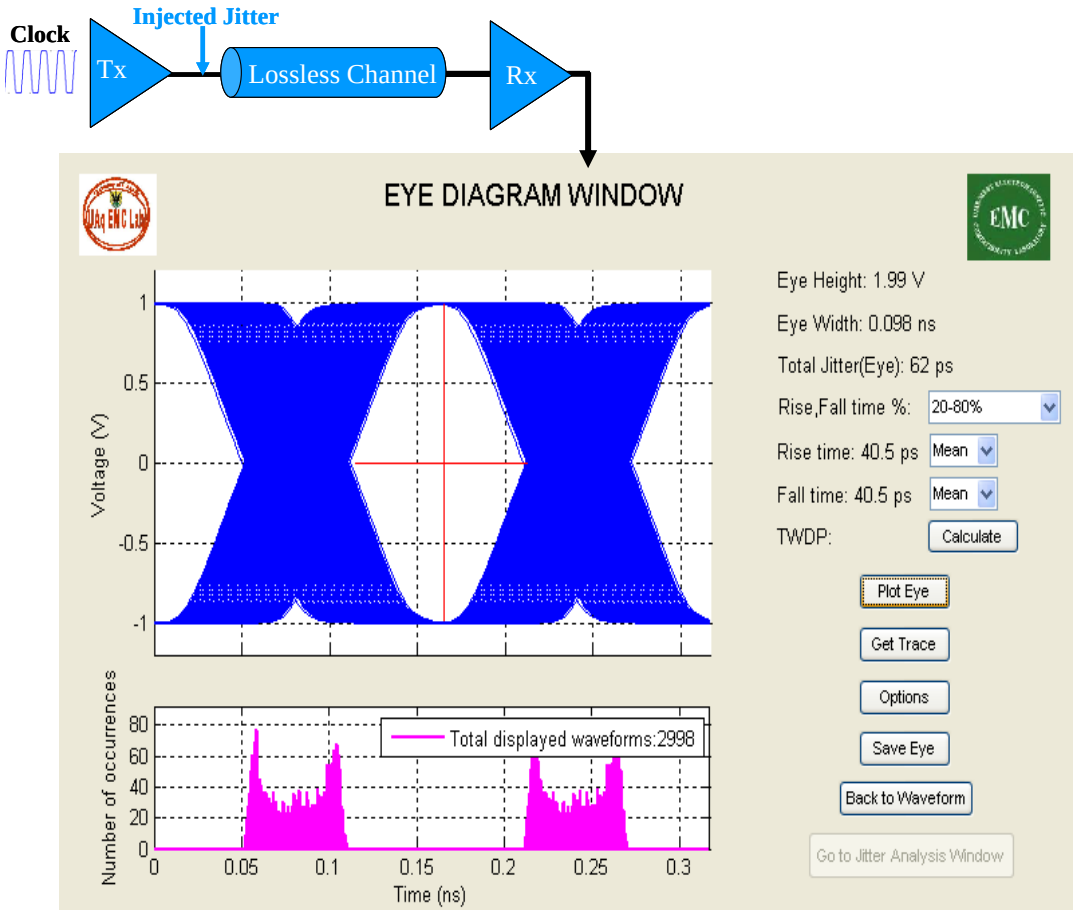

Figure 3.6. Eye diagram and histogram for injected jitter of PJ=50ps and RJ=2ps

3.3. DCD INJECTION

In the tool, DCD injection is modeled as a voltage offset. In real-time scopes and sampling scopes, the jitter analysis measurements often registers a DCD jitter, mainly due to offset shifts in the signal used in transmission at the output of Tx. The eye diagram is always measured at the reference level, which is the zero crossing of the signal. Because of the voltage offset, this zero crossing changes, and the change is reflected as a DCD in jitter analysis measurements. In the tool, to inject DCD an equation relating rise/fall time

and minimum value of voltage is derived by carefully analyzing the eye diagram. Based on the property of similarity of triangles, an equation is obtained for the amount of offset needed to inject a certain amount of DCD into the data stream at the output of Tx. Figure 3.7 depicts the triangular approximation and the derivation of the equation.

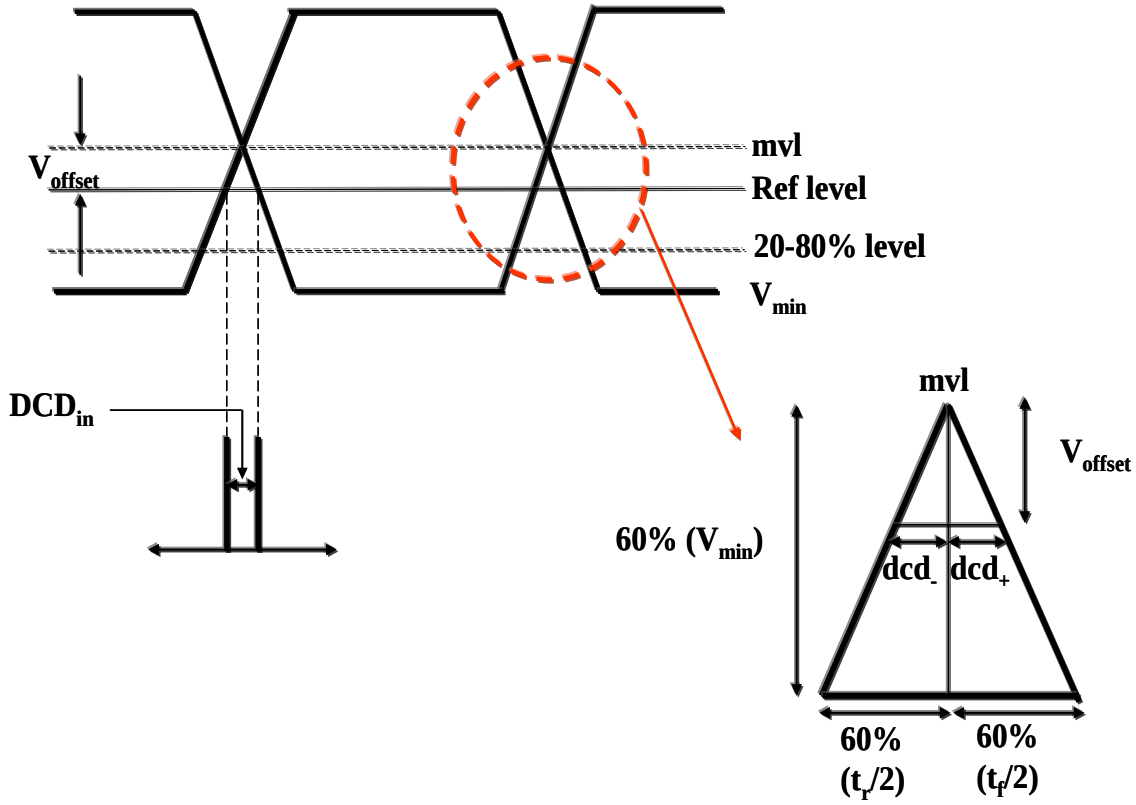

Figure 3.7. Triangular approximation of the eye to calculate offset needed to inject DCD

This derivation is illustrated as follows:

$$DCD_{injected} = DCD_{in} = dcd_{-} + dcd_{+} \tag{6}$$

$$DCD_{in} = \frac{tr * V_{offset}}{2 * V_{\min}} + \frac{tf * V_{offset}}{2 * V_{\min}} \tag{7}$$

$$DCD_{in} = \frac{(tr + tf) * V_{offset}}{2 * V_{\min}} \tag{8}$$

In equation 7, V_{offset} can be calculated since the amount of DCD to be injected (DCD_{in}), the rise/fall time (t_r/t_f), and the value of V_{min} are known. The term V_{offset} represents the voltage by which the signal at the output of Tx will be offset to get the amount of DCD specified by the user. To determine whether the DCD has been injected properly, a clock sequence distorted with DCD of 8ps is transmitted through a transmission line. DCD has an additive property when the total jitter at the input to Rx is analyzed. Since a lossless transmission line is used, rise/fall time does not degrade. Hence, the jitter monitored at the input to Rx should be the same as the injected DCD. Figure 3.8 shows the eye diagram and histogram screenshot from the link path analyzer tool. The histogram clearly shows a dual-dirac distribution with no distribution in between. The jitter recorded is 8.34ps, which is fairly close to injected DCD.

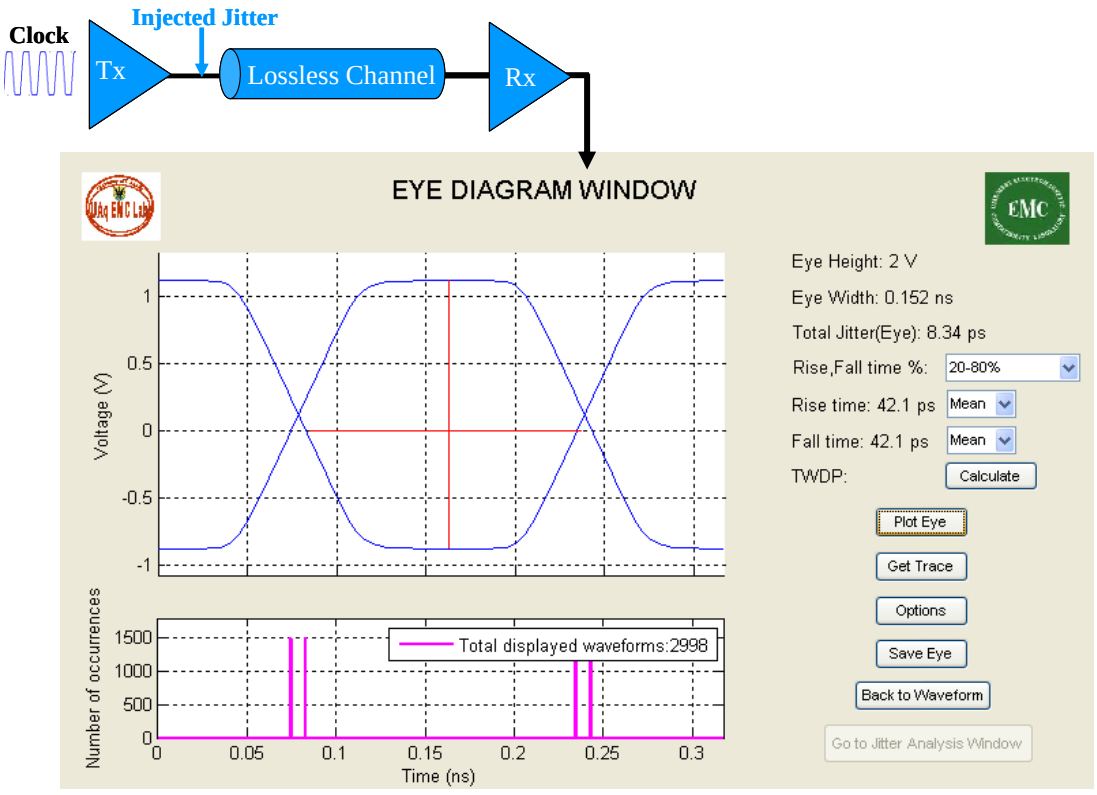

Figure 3.8. Eye diagram and histogram for injected jitter of DCD=8ps

3.4. ISI INJECTION

ISI does not have a specific mathematical model. To inject ISI into the system, a Matlab GUI was designed in the link path analyzer tool that designs a wide variety of filters. The user-designed filters include low-pass, high-pass, band-pass and band-stop filters. The parameters needed to design them are cut-off frequencies, order, and gain. User-obtained filters obtained from measurements can also be loaded to inject ISI to the output of Tx just before the actual channel under consideration. Figure 3.9 shows the GUI used to load the ISI filters.

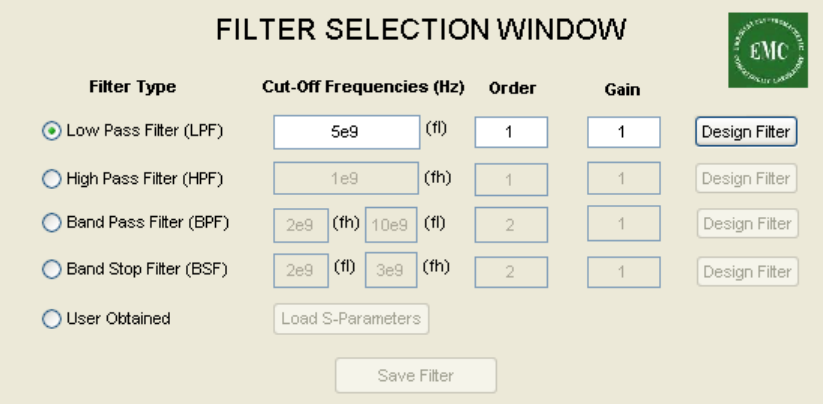

Figure 3.9. Matlab GUI that designs and loads the ISI filters

4. TIME-INTERVAL ERROR (TIE) AND JITTER SPECTRUM

A second goal of this research is to separate injected jitter components at the receiver input to study how they are affected by the channels. To separate jitter, one must understand how the components manifest themselves in the jitter spectrum. To get the jitter spectrum, computation of the jitter in the time domain on the waveform has to be done. This jitter can be computed as period jitter, cycle-cycle jitter, or time interval error (TIE) [6]. Figure 4.1 shows how these quantities relate to each other.

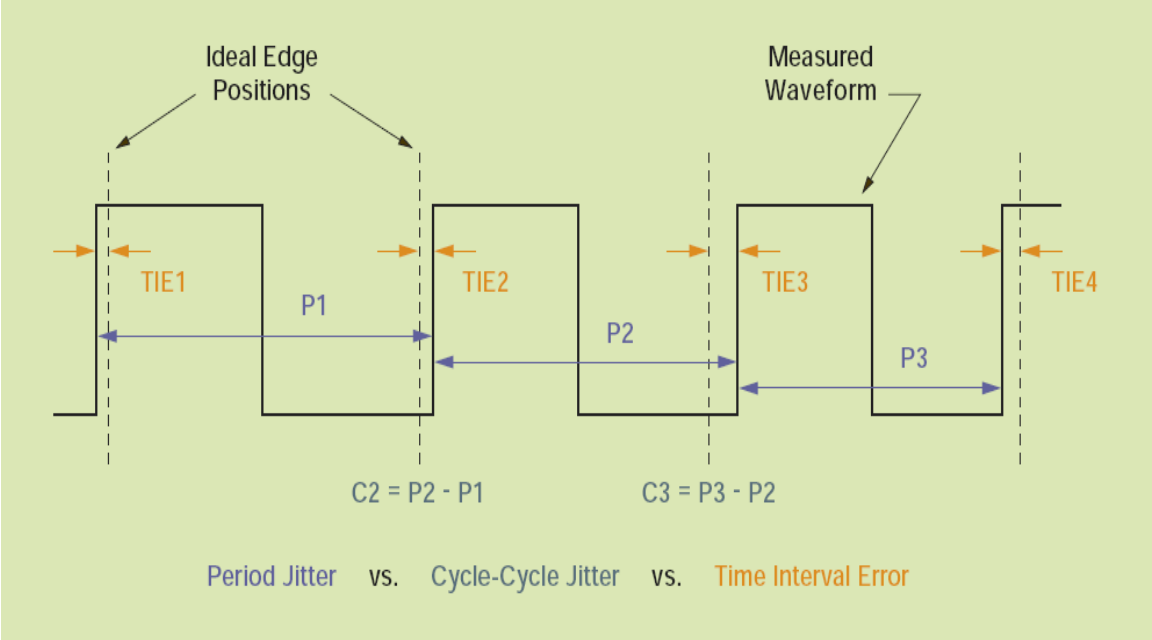

Figure 4.1. Periodic jitter, cycle-cycle jitter and time-interval error

Periodic jitter simply measures the period of the measured waveform. It is represented in Figure 4.1 by P1, P2 and P3. Cycle-cycle jitter measures the change in period of two adjacent cycles, as represented by C2 and C3. The TIE measures the zero crossing transitions of the measured waveform against its ideal counterpart. The ideal

counterpart is well represented by a jitter-free clock. This calculation is represented by TIE1, TIE2, TIE3 and TIE4. The present research used TIE to calculate the jitter spectrum on which combinations of spectral and mathematical analyses have been performed to separate out the jitter components.

4.1. CALCULATION OF TIE

Time interval error is the difference between the observed edge time and the expected edge time for each edge present in a data stream. Figure 4.2 shows how the TIE is calculated in the tool.

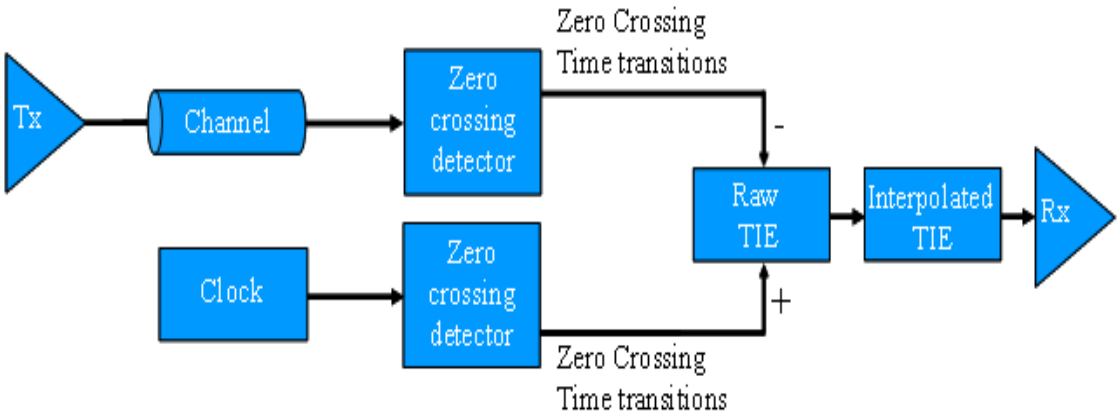

Figure 4.2. TIE calculation

The data waveform at the output of the Tx is delayed by the channel once it reaches the input to Rx. For the TIE calculation, this waveform must be aligned with the clock waveform; however this process can be circumvented in two ways.

First, the delay of the channel can be calculated, and the clock waveform can be delayed by the same amount while computing the TIE. The second approach, which is used in the tool, the clock waveform is transmitted along with the data waveform. The magic of clock is that no jitter will be introduced in it by ISI despite some amplitude

distortion. The clock waveform and data waveform are equally delayed, and edges can be compared to obtain the TIE.

To calculate the observed edge time, the edge time or zero crossing transition times of each edge in the data stream must be calculated. Each of these transitions must be compared with an ideal or expected edge time. For this purpose, a jitter-free clock is used. Its edge transitions or zero crossing transition times are also calculated. Finally, both of these are subtracted to get the raw TIE waveform.

A PRBS or fiber-channel sequence (CJTPAT, CRPAT) need not have a transition every bit period, although the clock does. In the absence of such transitions, any one of the available interpolation methods must be applied to the raw TIE waveform to fill in the spaces [7].

Figure 4.3 shows the entire process of determining the TIE waveform that is analyzed for the jitter components. The first portion of the figure plots the data waveform taken from the output of a channel. This waveform must be compared with an ideal counterpart, which is a clock waveform. The clock waveform is transmitted through the same channel. It suffers some amplitude distortion, but the edge positions do not change because the waveform is unaffected by ISI. The second portion of the figure shows the TIE values obtained from a comparison between the edge timings of the data and those of the clock. At some positions in the data waveform, no transitions occur. At the edges, where there are no data transitions, points in the raw TIE marked with an X are interpolated to yield the interpolated TIE. The tool used linear interpolation. The third portion of the figure shows the prediction of the TIE values at nontransition points. Finally, the TIE value at each point must be extended for an entire bit period. The fourth portion in the figure represents the TIE waveform.

The TIE waveform can be plotted in either of the two ways. First, the extended TIE values for each bit period can be plotted. Second, the TIE value can be plotted against each bit at which the edge transition is considered. In this case, the plot is called a TIE trend. The final portion of Figure 4.3 shows the TIE trend obtained by plotting the TIE value at each transition point of a bit. This type of plot analyzes the amount of data-dependent jitter contributed by each bit.

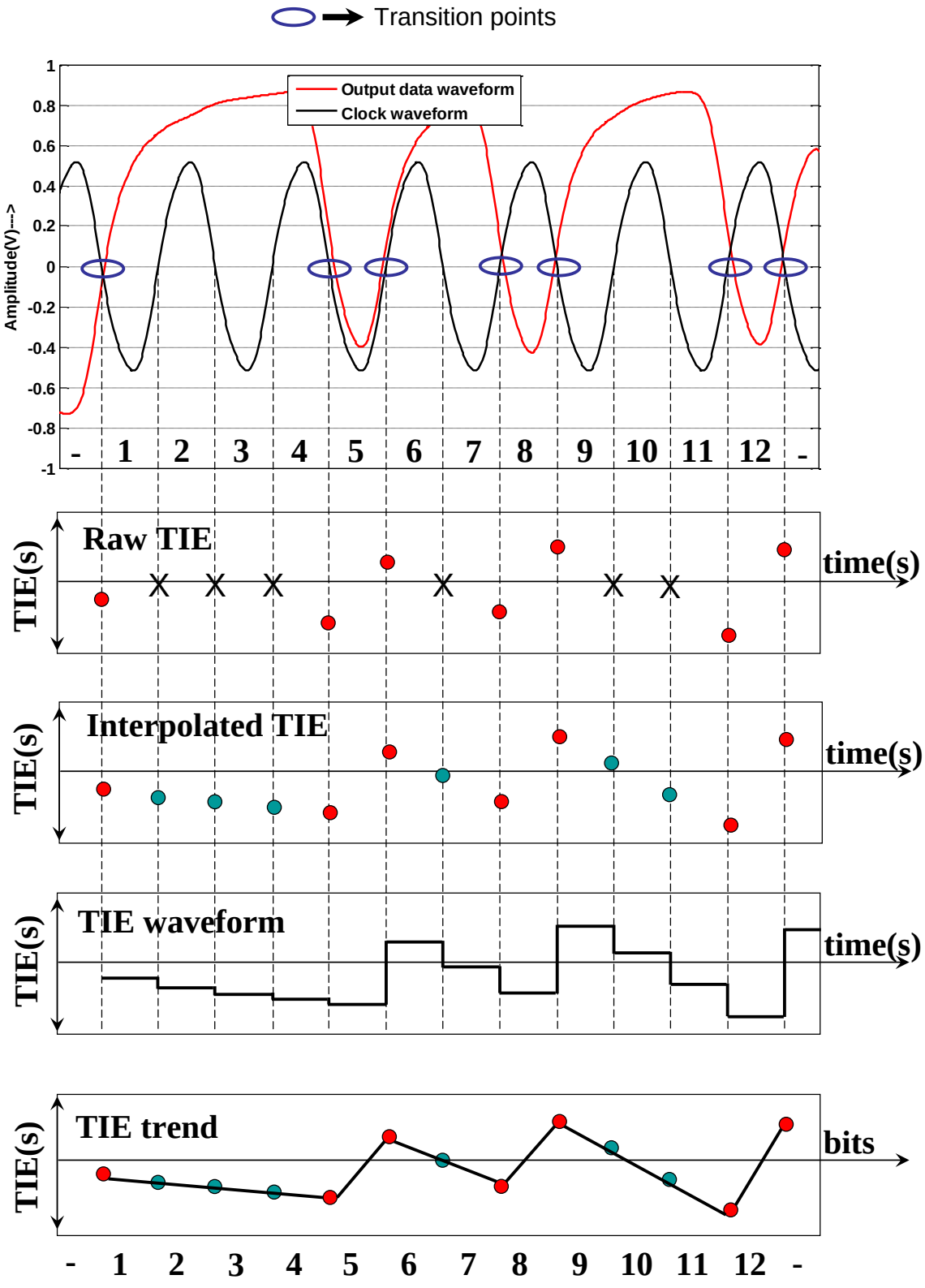

Figure 4.3. TIE waveform and trend

The peak-to-peak value of the TIE is the total jitter (TJ) at the BER, which inturn depends on the number of bits transmitted. An understanding of the manifestation of the combined jitter components in the TIE spectrum demands the study of the TIE trend of each jitter component. This work used clock-data waveform to analyze the TIE trend because the effect of ISI is not be reflected in this case. A lossless transmission line was used to prevent amplitude distortion of the waveform.

4.1.1. TIE of RJ. A clock-data waveform with 3000 bits, distorted with RJ of 1.2ps (rms) was transmitted through a lossless transmission line. During the TIE calculation, the distorted clock-data waveform is compared with a jitter-free clock. Since the clock-data waveform undergoes a transition every bit-period, no interpolation was required after calculation of the raw TIE. Figure 4.4 shows the TIE waveform for this case.

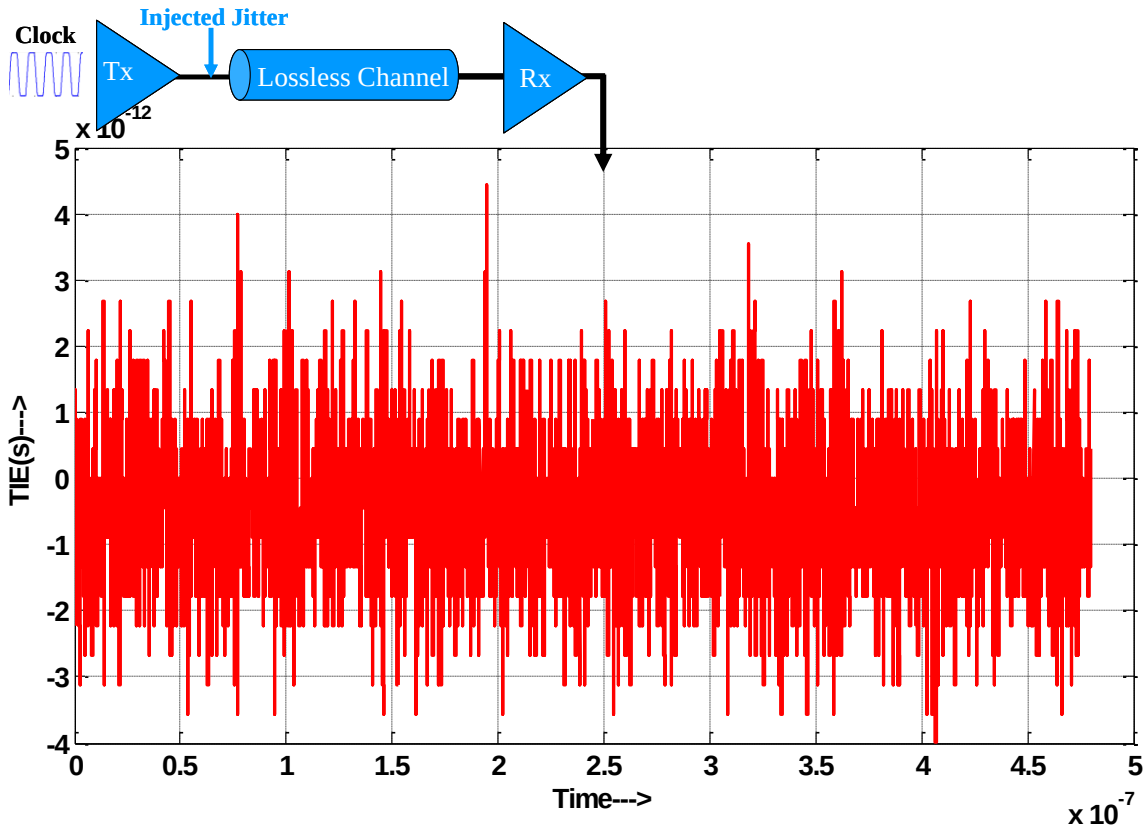

Figure 4.4. TIE of the waveform at Rx for injected jitter of RJ=1.2ps (rms)

The peak-to-peak value of the TIE yields TJ at the present BER. Assuming 1 error in 3000 bits, the BER is 1/3000 = 3.33e-4. The scaling factor to convert RJ_{rms} to RJ_{pp} can be calculated as:

$$\alpha = erfcinv(BER / DTD) * \sqrt{8}. \quad (9)$$

Data transition density is 100% for clock and 50% for other data. With a BER of 3.33e-4 and a DTD of 100%, α is equal to 7.1763. Thus, RJ_{pp} is equal to 7.1763 * 1.2ps, which in turn is equal to 8.612ps. The peak-to-peak value of the TIE is 8.88ps, which is fairly close to the calculated value. The TIE of RJ is a set of random numbers with Gaussian distribution because RJ injection by phase modulation causes random placements of edge timings.

4.1.2. TIE of PJ. A clock-data waveform with 3000 bits, distorted with PJ of 5ps is transmitted through a lossless transmission line. During the TIE calculation, the distorted clock-data waveform is compared with a jitter-free clock. Since the clock-data waveform undergoes a transition every bit-period, no interpolation is required after calculation of the raw TIE. Figure 4.5 shows the TIE waveform for this case.

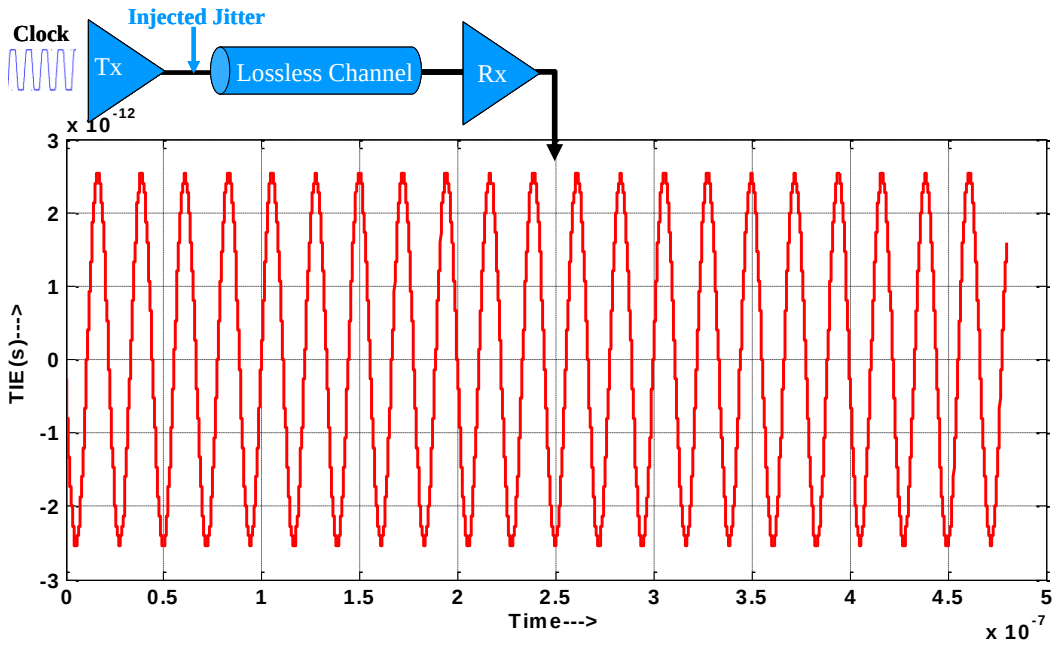

Figure 4.5. TIE of the waveform at Rx for injected jitter of PJ=5ps (peak-peak)

The peak-to-peak value of the TIE yields TJ which was 5.0669ps in this case, fairly close to the injected value of 5ps. The TIE of PJ is a periodic distribution, which in this case is sinusoidal, because PJ injection by phase modulation causes the edge timings to follow a periodic pattern.

4.1.3. TIE of DCD. The tool models DCD by adding a voltage offset equal to the amount of DCD required by the user. Unlike RJ, the TIE of DCD can be easily predicted. Figure 4.6 shows how the TIE is determined. When the offset is added, the medium voltage level (MVL) of the signal also shifts by the same amount, but the reference level at which the jitter is measured remains the same. During calculation of TIE, the edge time of the waveform at each edge is subtracted from the ideal edge time of the jitter-free clock. Since the ideal edge alternates between arrival before and after the data edge, calculated TIE varies between dcd_+ and dcd_-. The TIE waveform thus constructed is a square wave with a positive peak of dcd_+ and dcd_- and its peak-peak value is the DCD.

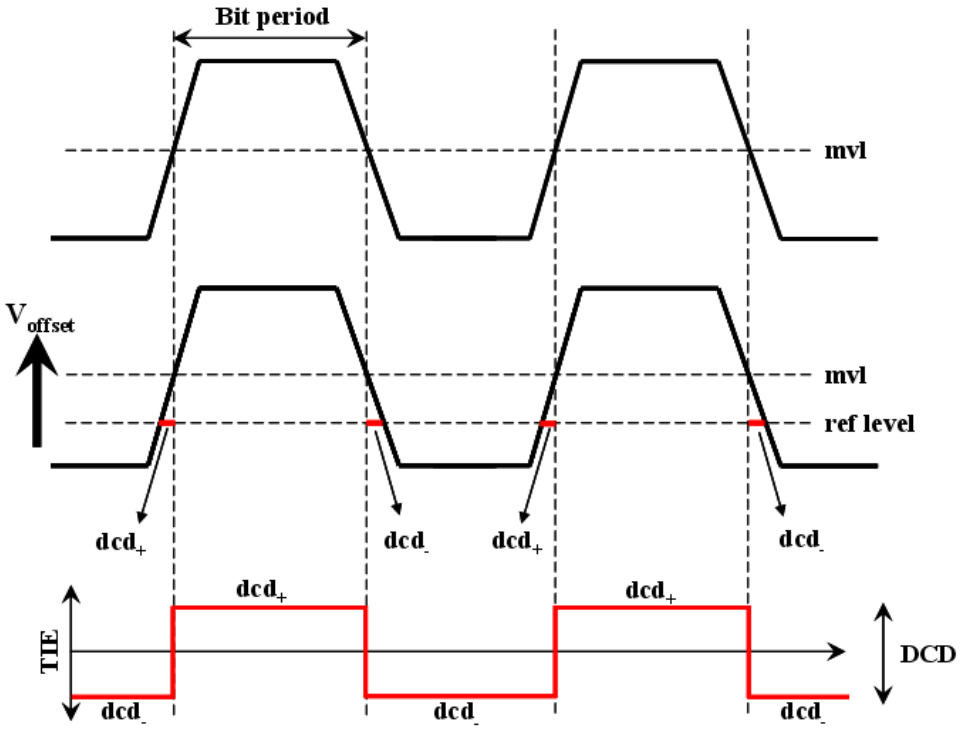

Figure 4.6. Determining TIE of DCD

A clock-data waveform with 3000 bits, distorted with DCD of 8ps is transmitted through a lossless transmission line. During the TIE calculation, the distorted clock-data waveform is compared with a jitter-free clock. Since the clock-data waveform undergoes a transition every bit period, no interpolation is required after calculation of the raw TIE. Figure 4.7 shows the TIE waveform for this.

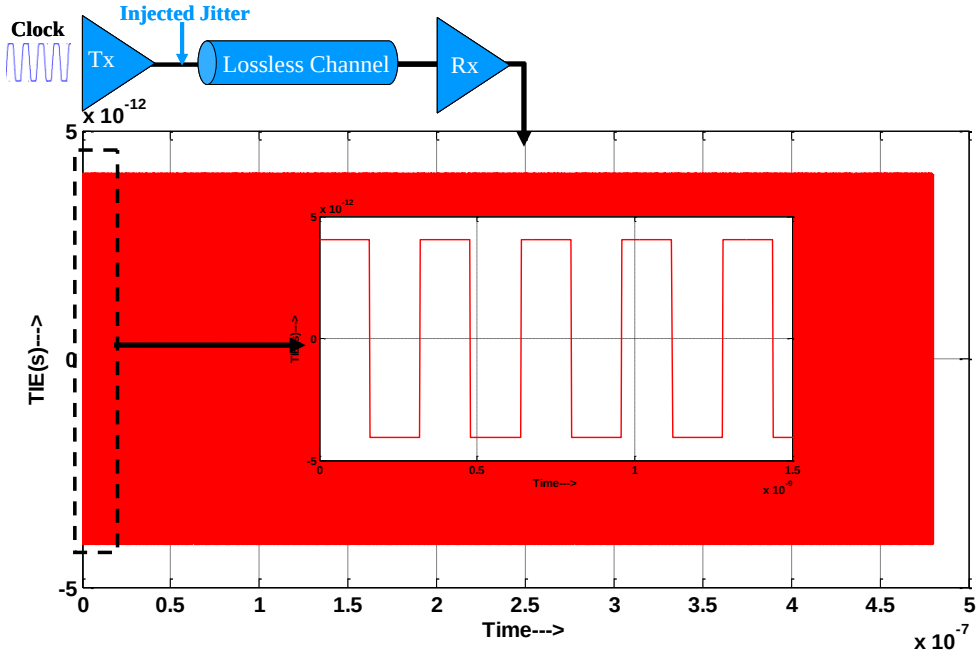

Figure 4.7. TIE of the waveform at Rx for injected jitter of DCD=8ps (peak-peak)

The peak-to-peak value of the TIE yields the TJ. In this case, the TJ was 8.0850ps, which is fairly close to the injected value of 8ps. The TIE of DCD will be a square wave.

4.2. TIE OF A PRACTICAL CASE

Using the process described above, this work confirmed the TIE trends of individual jitter components. RJ follows a random Gaussian distribution, PJ has a

sinusoidal distribution, and DCD has a square wave pattern trend. When all these jitter components are simultaneously injected into the data waveform (not a clock) and transmitted through a lossy transmission line, the TIE extracted at the receiver end follows a complex trend now also under the influence of ISI. However, a careful analysis of the TIE spectrum (obtained by performing an FFT) reveals that the jitter components appear at certain defined positions. Their appearance at these points would not have been possible if analyzed in the time domain. A PRBS-9 differential signal (~2550 bits) with differential voltage of $2V_{pp}$ and rise/fall time of 40ps (20-80%) is transmitted through a backplane channel at 6.25Gbps. Figure 4.8 shows the differential transfer S-parameter (Sdd21). This S-parameter is used wherever possible in the succeeding sections.

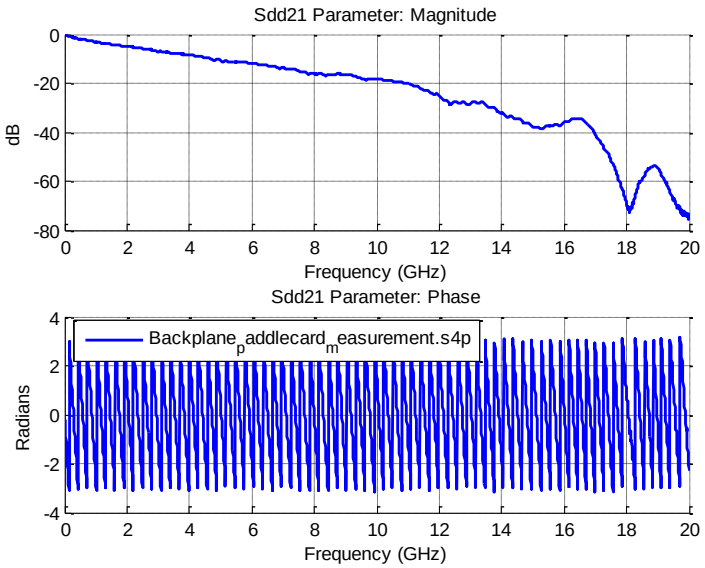

Figure 4.8. Sdd21 of the backplane channel used in transmission

The differential signal is distorted with an RJ (rms) of 1ps, PJ of 10ps at 20MHz, and a DCD of 3ps prior to transmission. PJ in a system is usually less than 5ps. An elevated value is taken to facilitate observation of its appearance in the TIE spectrum. A

TIE analysis is performed on the waveform at the receiver end; Figure 4.9 shows the trend and histogram.

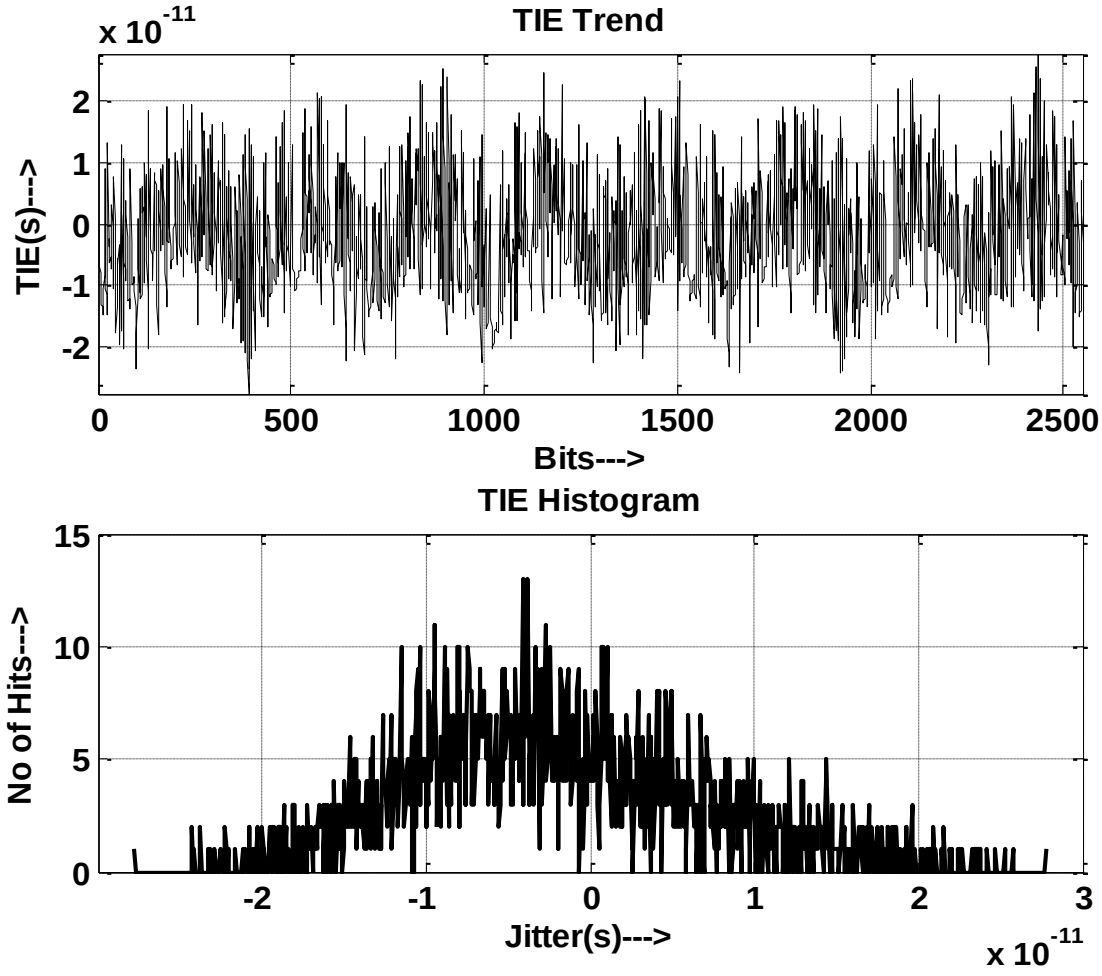

Figure 4.9. TIE trend and histogram of waveform at Rx

The TIE trend clearly shows a sinusoidal component representing PJ with a noise distribution riding on top. This is due to the high value of PJ chosen for the simulation. TJ obtained from the TIE is around 55.6ps, which is the contribution of RJ, PJ, DCD, and ISI. Figure 4.10 shows the TIE spectrum obtained by taking an FFT of the TIE.

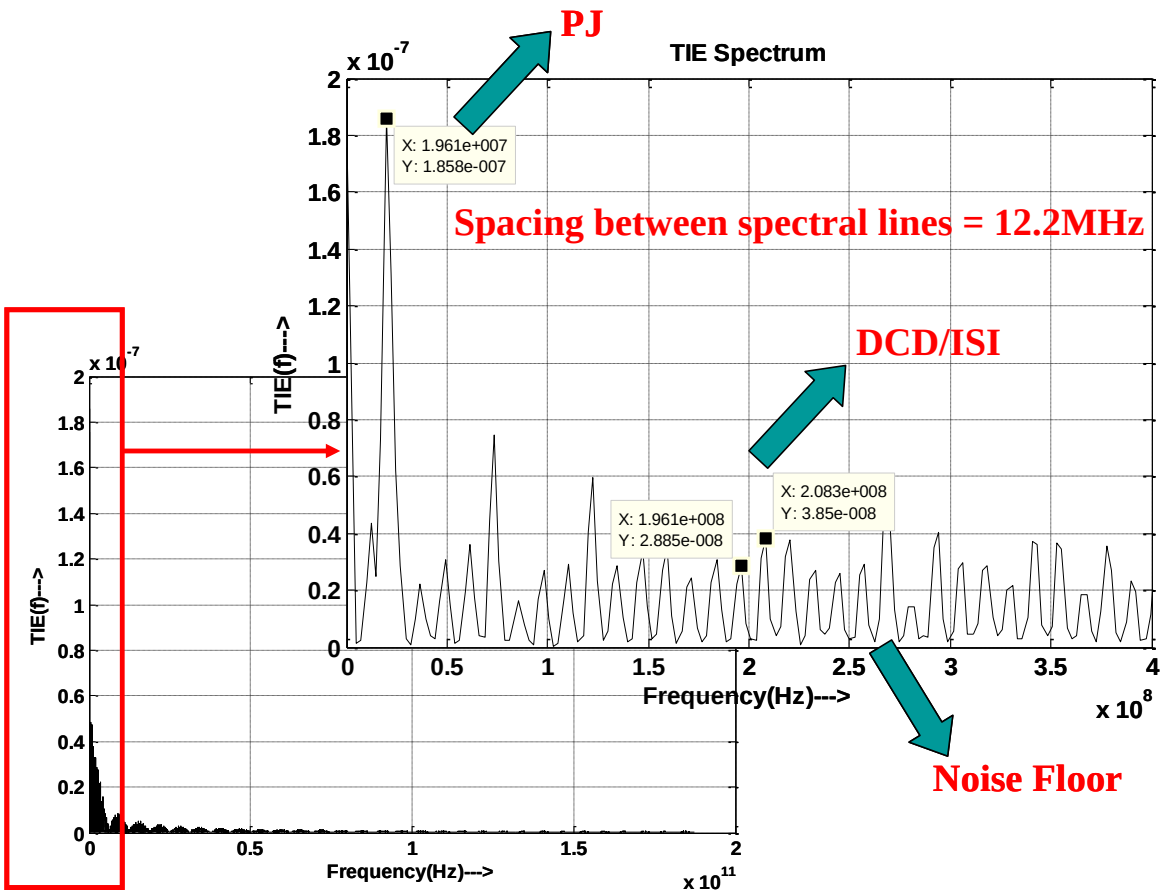

Figure 4.10. TIE spectrum

The TIE spectrum has a spectral component at 20MHz, which is the injected PJ. In addition to the noise floor, spectral components appear at integral multiples of Bit rate divided by the number of bits in one repetition. Since the number of bits in one repetition of PRBS-9 is 511 and the bit rate used is 6.25Gbps, the repetition rate is 6.25Gbps divided by (2^9-1) which in turn is equal to 12.2 MHz. These spectral components represent ISI and DCD. When the PJ value in the system is high, the spectral leakage in the TIE spectrum encloses some of the DCD/ISI components. An efficient windowing function must be adopted, or more bits must be taken to improve the resolution of the FFT data so that PJ and DCD/ISI components can be clearly differentiated. While performing jitter analysis real-time scopes from Tekronix use a peak detection algorithm

to mark the ISI/DCD bins and retain them only in the spectrum while setting all the other bins corresponding to PJ and RJ at zero. The IFFT on this modified spectrum yields the combined jitter caused by ISI and DCD. However at high bit rates and with the use of longer patterns such as PRBS-15 or PRBS-31, the pattern repetition rate becomes extremely slow. The FFT information thus becomes difficult to resolve, and the jitter components can be separated. For example, a PRBS-31 running at 10GE rate of 10.3125Gbps has DCD/ISI spectral components repeating at a pattern repetition rate of 10.3125Gbps divided by (2^{31}-1) which in turn is equal to 4.8 Hz [8]. All the problems addressed here have been considered in the development of a robust method of jitter decomposition. For dense spectrums from PRBS-7 onwards, this work proposes an ISI extraction method based on equalization and extrapolation.

5. JITTER DECOMPOSITION

Spectral leakage and resolution are the two main issues that prevent the differentiation of the various jitter components in the TIE spectrum. When PJ is high, it submerges the low frequency DCD/ISI spectral components. This effect can be remedied by using a proper windowing function on the TIE prior to taking its FFT. When the PJ spectral line is very close to the DCD/ISI spectral components, separating them is very difficult. This resolution issue can be solved by taking more bits. Most of the instruments in the industry use a dual-dirac model approximation on the histogram of the jitter spectrum to perform the initial separation of deterministic jitter (DJ) and random jitter (RJ) [9]. The value of RJ is determined using a tail-fitting algorithm that attempts to place Gaussian fits on both tails of the histogram. The average of the standard deviation of the best Gaussian fit on both tails is the rms value of RJ. In many cases, the method is not successful in getting tails to fit at both ends of the histogram. Further, when the channel is lossy, under the influence of ISI the histogram becomes so complicated that it is difficult to apply the dual-dirac model approximation to remove the DJ and RJ. Thus, the tail-fitting algorithm is not an effective method to calculate RJ.

The jitter decomposition process developed in this research uses the unique properties of clock. Clock waveform is not affected by ISI. Also, the spectrum of the clock has spectral lines occurring only at odd intervals. The pattern spectrum of the clock is closely related to the TIE spectrum, making the TIE spectrum of clock easy to work with for the separation of PJ and RJ. In addition, PJ and RJ are not affected by channel properties since they are uncorrelated to the data. A data waveform and clock waveform distorted by the same amount of PJ and RJ passed simultaneously through the same channel yield the same value of PJ and RJ when decomposed at the input to Rx. In the decomposition algorithm, the data line is used for DCD and ISI decomposition, whereas the clock line is used for PJ and RJ decomposition. Figure 5.1 shows the protocol. A high-speed Bertscope from SyntheSys Research, Inc., relies on a similar principle in their jitter triangulation software when decomposing the jitter components. This instrument uses a short pattern (e.g., clock) to decompose RJ, PJ, and DCD. Once these values are

obtained, they are locked in the jitter software. A long pattern is then used to obtain the ISI caused by the channel. This step is based on the assumption that the PJ and RJ do not change when a change is made from a short pattern to a long pattern.

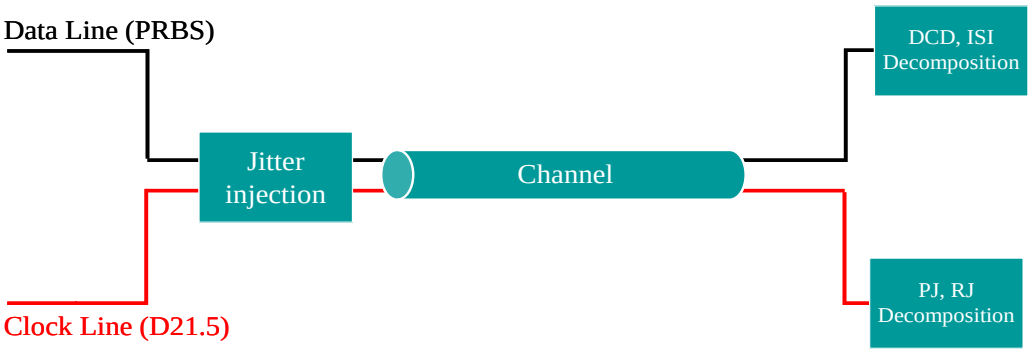

Figure 5.1. Jitter decomposition protocol

5.1. PJ DECOMPOSITION

As specified by the decomposition protocol, PJ is separated from the clock line. Both the clock and data lines are distorted by the same jitter values. A PRBS-9 differential signal with a differential voltage of $2V_{pp}$ and rise/fall time of 40ps (20-80%) is transmitted through a backplane channel at 6.25Gbps. The differential voltage that represents the data and hence the clock is distorted by PJ of 2ps at 10 MHz, RJ of 1ps (rms), and DCD of 3ps. Figure 5.2 explains the PJ decomposition algorithm. A TIE calculation is performed on the waveform at the output of the channel. To detect the position of the PJ spectral line in the TIE spectrum and its frequency, the effect of the RJ and DCD must be nullified. Autocorrelation is performed to remove the nonperiodic components (RJ and DCD), leaving behind periodic variations caused by PJ. Windowing is applied after autocorrelation to reduce spectral leakage. This work used a hanning window for this purpose. The spectrum of the autocorrelation result is obtained by taking an FFT. Ideally, the spectrum should contain only one spectral line corresponding to the PJ, as shown in Figure 5.3, which includes only the first 200 bins.

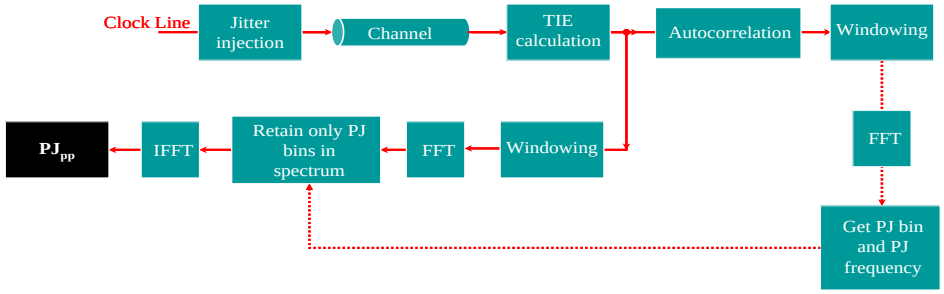

Figure 5.2. PJ decomposition algorithm

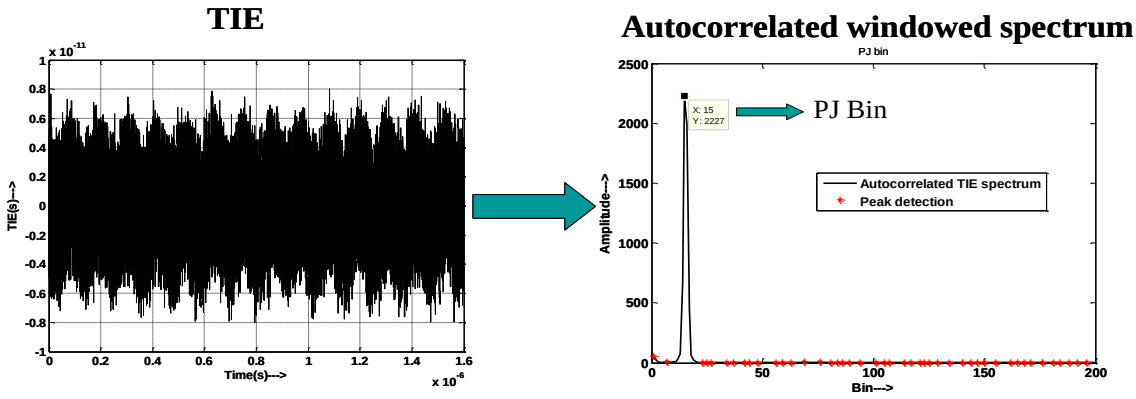

Figure 5.3. Autocorrelated windowed spectrum showing the PJ bin

Artifacts above 100 MHz are usually disregarded since PJ is prevalent at low frequencies. Peak detection is performed to obtain this bin. Autocorrelation cannot give the actual amplitude of the PJ, but it gives the position of the PJ in the TIE spectrum, along with the PJ frequency. Once the bin is obtained, another set processing is done on the TIE. The TIE is windowed, and the jitter spectrum is obtained. In the TIE spectrum, only the bin obtained from the autocorrelated spectrum results is retained; all the other bins are set to zero. An IFFT is taken on the modified spectrum to get a TIE corresponding to PJ. The peak-to-peak value of this TIE is taken. Figure 5.4 shows how the PJ is isolated from the TIE.

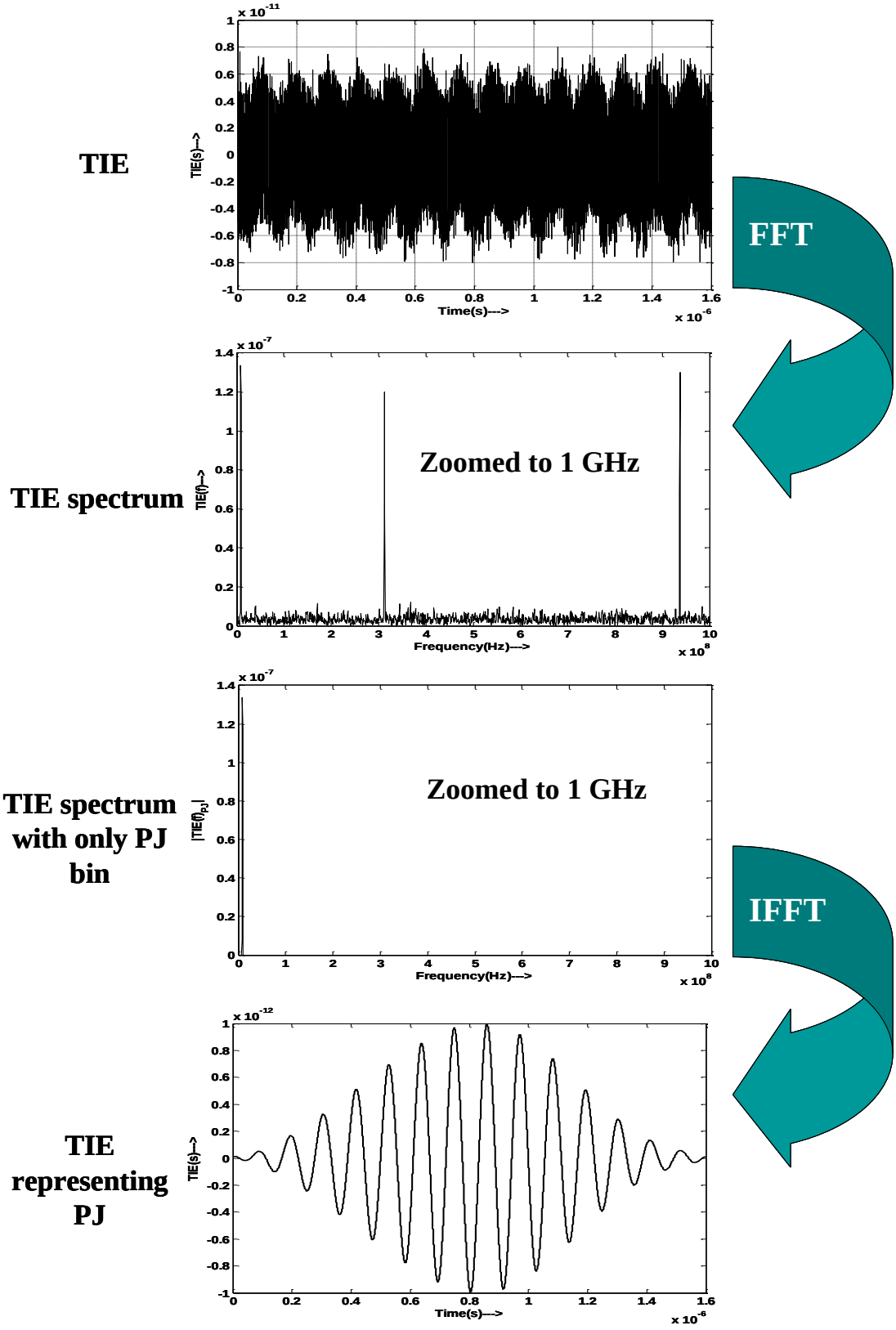

Figure 5.4. Isolation of PJ from TIE

The PJ is 2.05ps, which is close to the injected value of 2ps, indicating that it should not be changed by channel effects.

5.2. RJ DECOMPOSITION

As specified by the decomposition protocol, RJ is separated from the clock line. Both the clock and data lines are distorted by the same jitter values. A PRBS-9 differential signal with a differential voltage of $2V_{pp}$ and rise/fall time of 40ps (20-80%) is transmitted through a backplane channel at 6.25Gbps. The differential voltage that represents the data and hence the clock is distorted by PJ of 2ps at 10 MHz, RJ of 1ps (rms), and DCD of 3ps. Figure 5.5 explains the RJ decomposition algorithm.

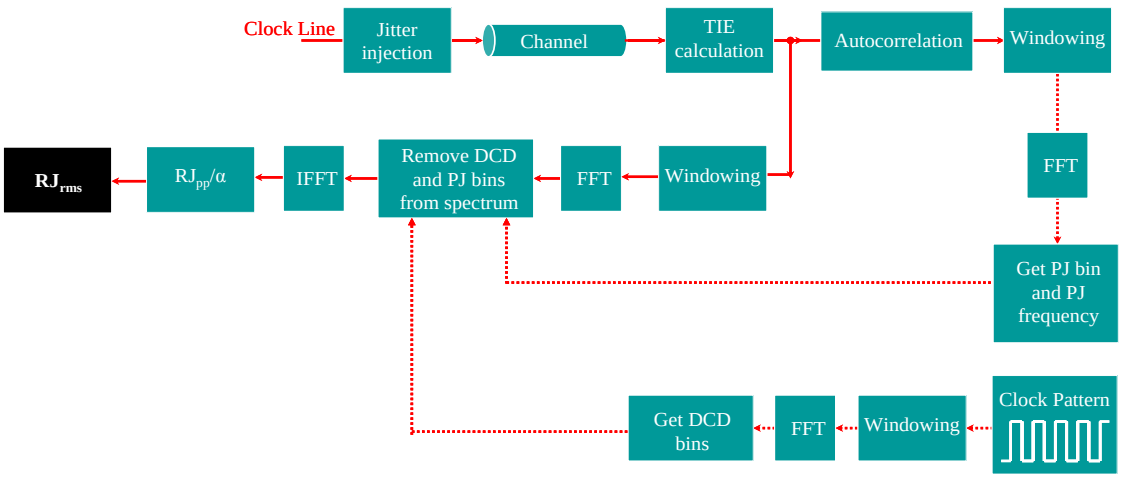

Figure 5.5. RJ decomposition algorithm

To detect RJ, the effects of PJ and DCD must be nullified from the TIE spectrum. This process involves detecting and removing the PJ and DCD bins from the spectrum and taking an IFFT on the modified version to get the RJ. To detect the PJ bin, the decomposition protocol for PJ is used. Autocorrelation is performed to remove the non periodic components (RJ and DCD) and leave behind periodic variations caused by PJ. Windowing is applied after autocorrelation to reduce spectral leakage. The spectrum of

the autocorrelation results is obtained by taking an FFT. Ideally, the spectrum should contain only one spectral line corresponding to the PJ. Artifacts above 100 MHz are usually disregarded since PJ is prevalent at low frequencies. Peak detection is performed to obtain this bin. Autocorrelation cannot give the actual amplitude of the PJ; however, it gives the position of the PJ in the TIE spectrum, along with the PJ frequency. Detection of the DCD bins involves use of the clock pattern. The spectrum of clock pattern has spectral lines repeating at odd intervals. The location of these bins in the clock spectrum matches the positions of the DCD bins in the TIE spectrum. The clock pattern is windowed prior to taking FFT to reduce spectral leakage. This work used a hanning window for this purpose. Using peak detection, the DCD bins are determined. Figure 5.6 shows the DCD bins obtained by taking an FFT of the pattern. The TIE waveform obtained from the TIE calculation is now windowed and converted to frequency domain using FFT. In this spectrum, the bins corresponding to PJ and DCD are set to zero, and the others are retained.

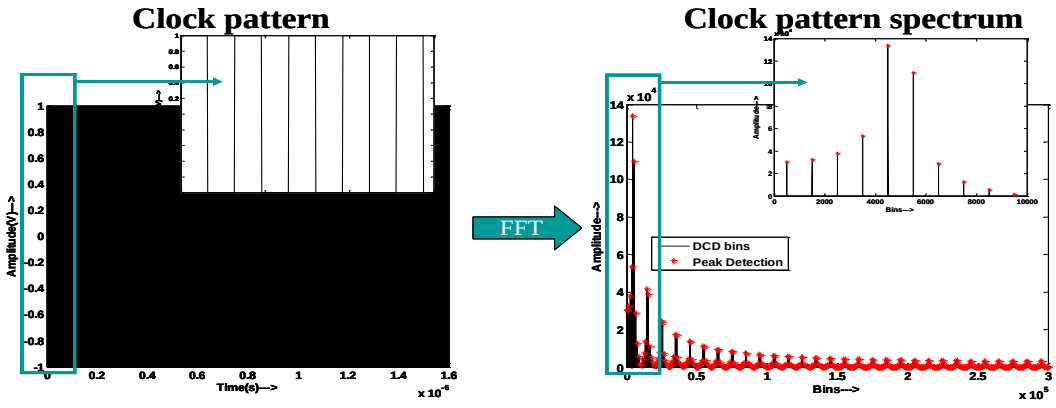

Figure 5.6. Clock pattern spectrum with DCD bins

An IFFT is taken on this modified spectrum to yield a TIE that should have only the contribution of RJ. The peak-to-peak value of the TIE should give the RJ_{pp}, which is 7.8651ps. Figure 5.7 illustrates the process of isolating RJ from TIE.

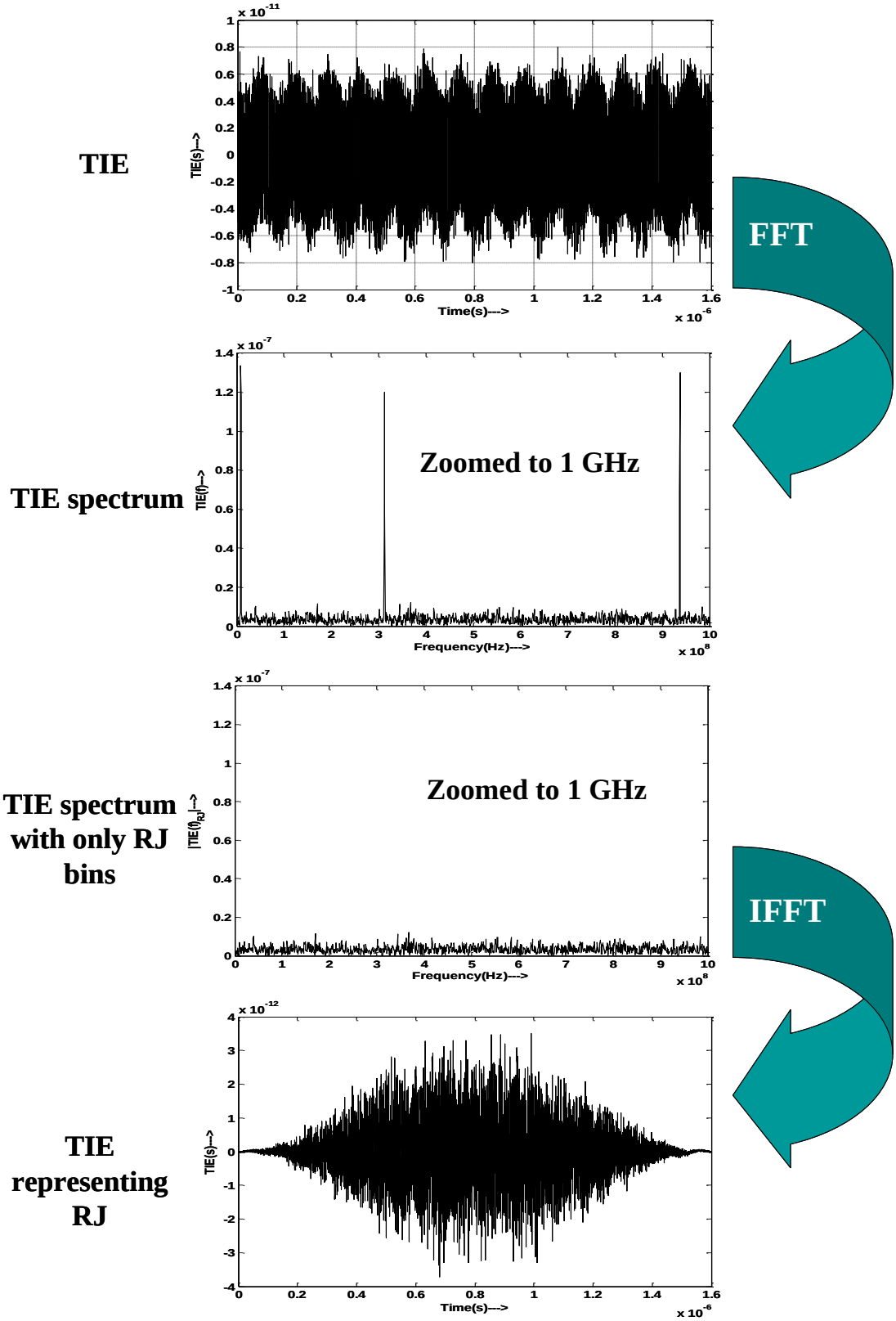

Figure 5.7. Isolation of RJ from TIE

To convert RJ_{pp} to RJ_{rms}, the former must be divided by the scaling factor corresponding to the number of bits taken. Since this simulation assumed 10000 bits of clock, the assumption of 1 error in 10000 bits gives a scaling factor of α which is equalt to 7.7812. RJ_{rms} is 1.01ps, which is almost the same as the injected value of 1ps, indicating that RJ is not affected by channel properties.

5.3 DCD DECOMPOSITION

As specified by the decomposition protocol, DCD is separated from the data line. To decompose the DCD at the input of Rx, the triangulation approximation equation used to inject the DCD at the output of Tx is used with some modifications. Figure 5.8 depicts the triangular approximation and the derivation of the equation.

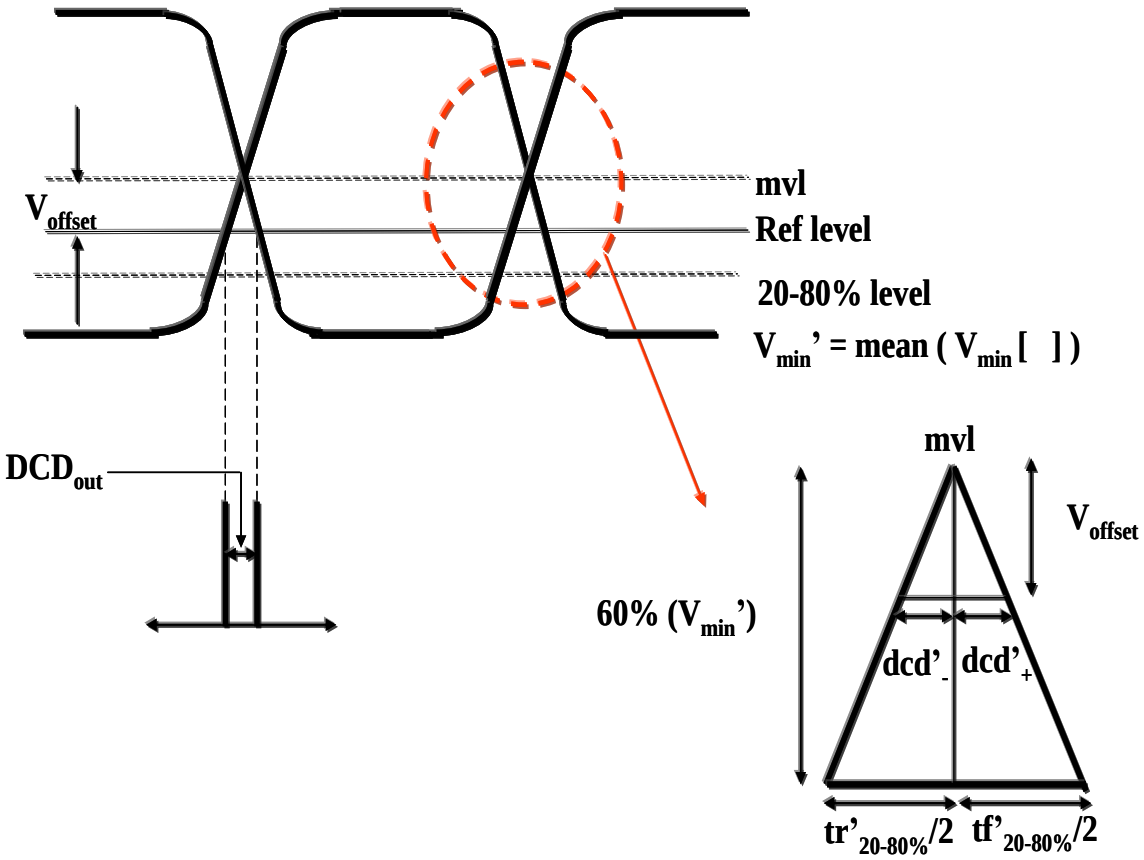

Figure 5.8. Triangular approximation of the eye to calculate DCD at the input of Rx

For simulation purposes, a PRBS-9 differential signal with differential voltage of $2V_{pp}$ and rise/fall time of 40ps (20-80%) is transmitted through a backplane channel at 6.25Gbps. The differential voltage that represents the data is distorted by PJ of 2ps at 10 MHz, RJ of 1ps (rms), and DCD of 3ps. At each transition point, the differential waveform will span a range between 1V and -1V, and the rise/fall time (20-80%) measured at this point is 40ps. These data do not change if a calculation is made at all transition points. The same cannot be said after the waveform goes through the channel. The effect of ISI varies depending on the pattern combinations present in the data waveform. In such a situation, measurement at all possible transition points yields a range of results. A long set of 0's following a long set of 1's (…..1111100000…...) spans the maximum but does not reach 1V (or -1V). The rise/fall time measurement for this pattern combination is the maximum. On the other hand, a single 0 preceded and succeeded by long set of 1's (…..11111011111…..) spans the minimum. The rise/fall time measurement for this case is the minimum. This work developed a code for performing these calculations at all transition points. The negative trends in voltage spans are accumulated in a variable V_{min} [ ]. The mean of the values accumulated in this variable is used in the calculation of DCD. The rise/fall time calculation includes the minimum, mean, and maximum values, and it is incorporated in the eye-diagram window of the link path analyzer tool. Mean rise/fall time is selected in the calculation of DCD. Figure 5.9 shows the GUI screenshot for this simulation.

The equation for decomposition of the DCD relies on the property of similarity of triangles. Equations 10, 11, and 12 show this derivation.

$$DCD_{decomposed} = DCD_{out} = dcd'_{-} + dcd'_{+} \tag{10}$$

$$DCD_{out} = \frac{tr'_{20-80\%} * V_{offset}}{2 * 0.6 * V_{\min}'} + \frac{tf'_{20-80\%} * V_{offset}}{2 * 0.6 * V_{\min}'} \tag{11}$$

$$DCD_{out} = \frac{(tr'_{20-80\%} + tf'_{20-80\%}) * V_{offset}}{2 * 0.6 * V_{\min}'} \tag{12}$$

Decomposed DCD is calculated to be 8.23ps after plugging in the values for mean rise/fall time and the mean of the negative trending spans. V_{offset} is the amount of offset

seen in the waveform at the input to Rx; it is the reference level at which TJ is measured. DCD increases after passing through the channel because of the degradation in rise/fall time and voltage amplitude. In fact, DCD increases because of the ISI induced on the data waveform by the channel.

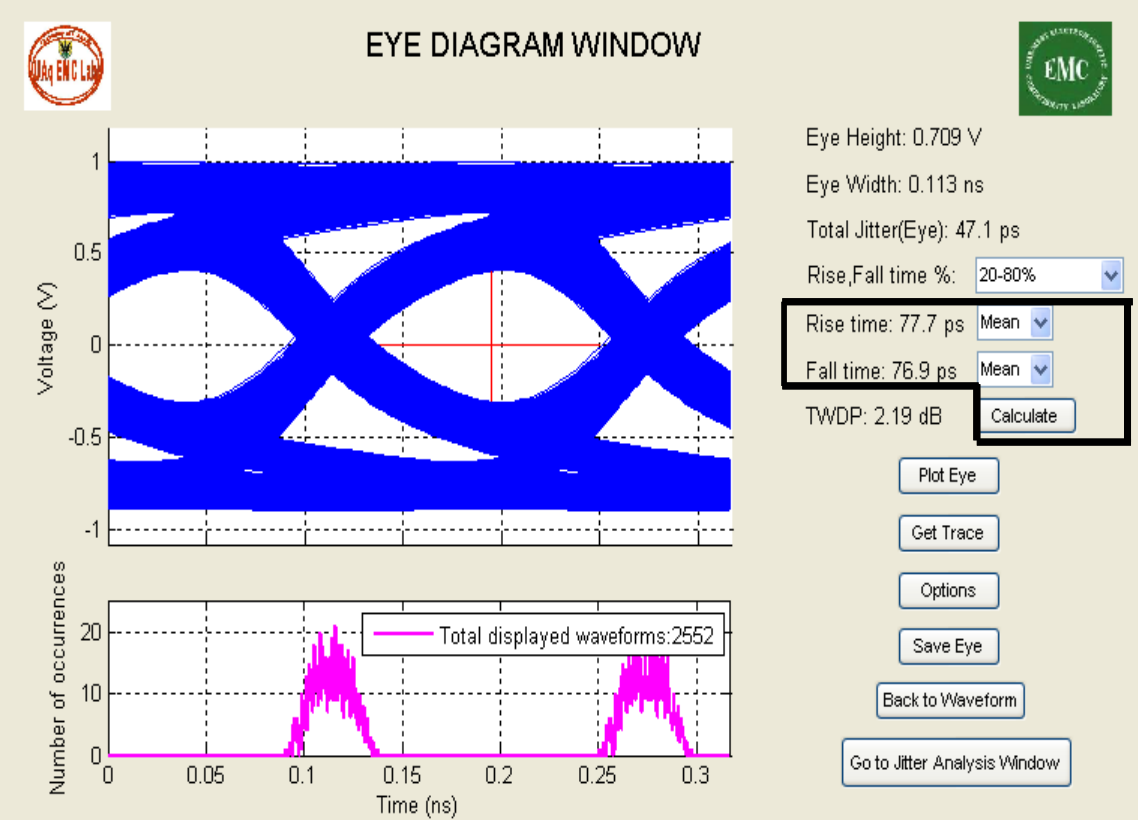

Figure 5.9. Eye-diagram GUI with rise/fall time calculation

5.4 ISI DECOMPOSITION

ISI is separated from the data line as a consequence of the decomposition protocol. As mentioned in Section 4.2 above, while measuring ISI and DCD, commercial real-time scopes separate the ISI/DCD spectral lines from the jitter spectrum and perform an IFFT to obtain the sum of DCD and ISI. Identifying the spectral lines becomes difficult when the pattern repetition rate is slow like in the case of PRBS-31. To

decompose ISI, this work proposes a separation technique based on the use of equalizers. When a signal goes through a channel, it becomes distorted due to ISI. The signal quality can be recovered by applying correction techniques at the transmitter and receiver. When such techniques are applied at the transmitter, the process is referred to as pre-emphasis [10]. Application to the receiver side is called equalization. These methods attempt to open the eye by nullifying the effect of the channel on the signal. The channel contributes primarily to ISI. Two main equalizer principles are used in this regard based on whether or not the user knows the channel properties. This work includes no detailed description of the equalizer theory. The jitter analysis GUI in the link path analyzer tool displays decomposed ISI values based on both principles.

In the link path analyzer tool, the user has access to the S-parameter used as a channel. When this S-parameter is cascaded with a channel having an inverse transfer response, the cascaded response has a magnitude of 1 (0dB) at all frequency values. Thus, the signal passes through the systems unaffected, and ISI is removed. The equalizer is designed to have the inverse transfer response. This simple principle forces the ISI to zero; it is referred to as a zero-forcing equalizer, and it is easy to implement provided the user has access to the S-parameter. The ISI values decomposed by this method do not depend on whether or not the S-parameter responses are linear, and they agree well most of the time. Figure 5.10 depicts the zero-forcing principle used to decompose the ISI.

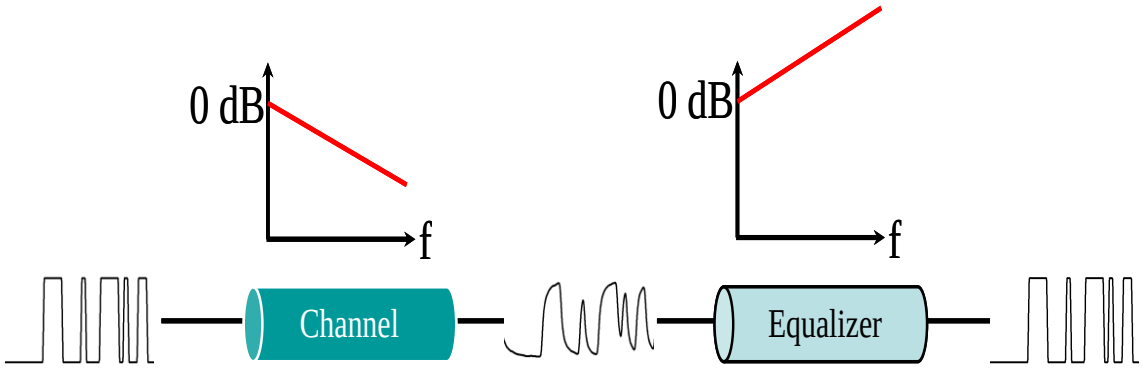

Figure 5.10. Zero-forcing method to nullify ISI

In most cases, the user has no access to the channel responses. Scopes have the option of performing jitter analysis on a waveform acquired from unknown sources. In such a case, it is not easy to predict the equalizer response that would counteract the ISI. A minimum mean square error decision feedback equalizer (MMSE-DFE) design obtained from appendix G of SFF-8431 standards was used here to acquire the taps needed to construct the equalizer response. The equalizer has feed-forward taps and feed-back taps; when these are, they attempt to open the eye at the input of the slicer, as shown in Figure 5.11. The ISI values decomposed by this approach depend on the linearity of the channel and do not work well if the response has stub resonances. This approach does generally give good results.

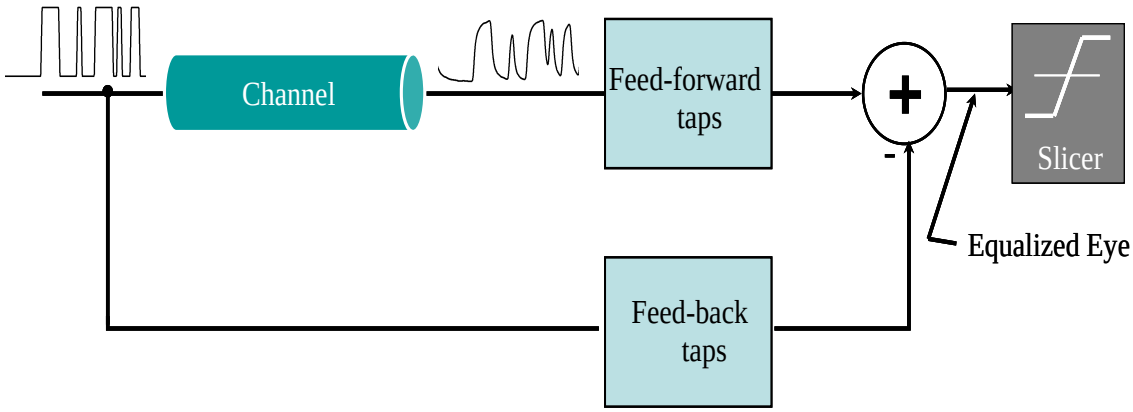

Figure 5.11. MMSE-DFE approach to obtain equalized eye

For simulation purposes, a PRBS-9 differential signal with a differential voltage of $2V_{pp}$ and a rise/fall time of 40ps (20-80%) is transmitted through a backplane channel at 6.25Gbps. The differential voltage that represents the data is distorted by PJ of 2ps at 10 MHz, RJ of 1ps (rms), and DCD of 3ps. Figure 5.12 shows the unequalized eye and the equalized eye with BER mapping.

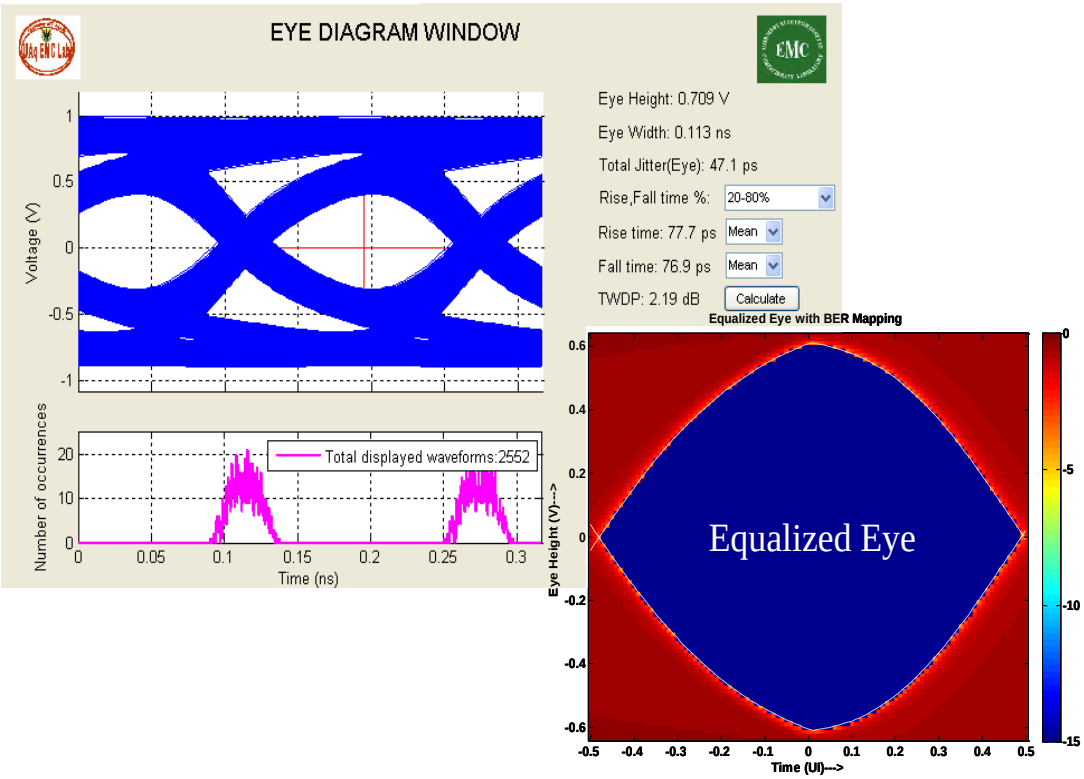

Figure 5.12. Equalized eye-diagram with BER Mapping

Assuming no crosstalk, the difference in TJ at equalizer output from that at channel output should give the value of ISI. The ISI obtained from this difference is underestimated because the channel output and equalizer output are at different BERs. To correct this, the protocol shown in Figure 5.13 is adopted here. From the channel output, the DCD is removed by canceling the offset in the signal. This signal now acts as the input to the equalizer. The equalizer can be either of the types discussed in Section 5.4 above. The TJ at channel output and equalizer output are calculated along with the corresponding BERs. Let the TJ at the channel output be represented as TJ_{out} and that at the equalizer output be represented as $TJ_{equalizer}$. The TJ at the equalizer output should ideally be same as the distorted input signal at the output of Tx. Let the BERs be represented as $BER_{channel}$ and $BER_{equalizer.}$ The corresponding scaling factors can be calculated from equation 9; let these be represented by $\alpha_{channel}$ and $\alpha_{equalizer}$. The RJ_{rms} and

PJ_{pp} at the channel output and equalizer output should not change because they are uncorrelated to the data. The initial TJ values are represented following:

$$TJ_{channel} = (\alpha_{channel} * RJ_{rms}) + PJ_{pp} + ISI \tag{13}$$

$$TJ_{equalizer} = (\alpha_{equalizer} * RJ_{rms}) + PJ_{pp} \tag{14}$$

Both these TJ values are then extrapolated to the industry standard BER of 1e-12 or 1e-14 using the bathtub curve. The scaling factor to extrapolate to 1e-12 is 14.1. Finally, both these extrapolated values are subtracted to obtain the actual ISI of the channel. The value obtained by this method tends to be about 1 to 2ps exaggerated but is well within standards. The extrapolation (to 1e-12) is represented by:

$$TJ_{channel(extrapolated)} = TJ_{channel} + [(14.1 - \alpha_{channel}) * RJ_{rms}] \tag{15}$$

$$TJ_{equalizer(extrapolated)} = TJ_{equalizer} + [(14.1 - \alpha_{equalizer}) * RJ_{rms}] \tag{16}$$

The ISI is given:

$$ISI = TJ_{channel(extrapolated)} - TJ_{equalizer(extrapolated)} \tag{17}$$

The ISI thus obtained is 35.5ps using the zero-forcing approach and 37.1ps using the MMSE- DFE method.

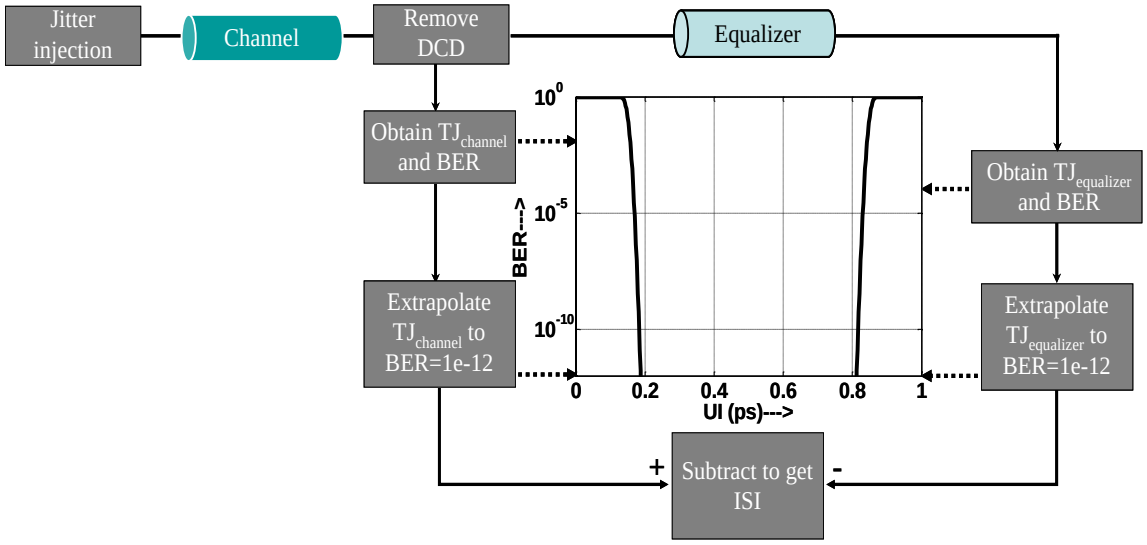

Figure 5.13. Extrapolation protocol to obtain ISI

The ISI for a clean PRBS-9 through the same channel is 34.5 ps. The increase can be attributed to the increase in ISI due to DCD injection and to exaggeration due to the proposed extrapolation method.

5.5 JITTER ANALYSIS GUI

The GUI for the jitter analyzer in the link path tool was designed based on the features of scopes from Tektronix, LeCroy, and Agilent. Real-time scopes can plot TIE trend, histogram, and spectrum. Both sampling scopes and real-time scopes plot bathtub curves. The tool includes codes for TIE calculation and bathtub curves. It shows the decomposed jitter values and plots all the parameters indicated above at three different test points, providing information about the transformation of jitter passing through them. For simulation purposes, a PRBS-9 differential signal with a differential voltage of $2V_{pp}$ and a rise/fall time of 40ps (20%-80%) is transmitted through a backplane channel at 6.25Gbps. The differential voltage that represents the data is distorted by PJ of 2ps at 10 MHz, RJ of 1ps (rms), and DCD of 3ps. Figure 5.14 displays the jitter analysis GUI with the jitter values obtained using the proposed decomposition methods and the plotting options in the tool. The simulation did not include ISI injection; therefore, the jitter values at TP2 match those at TP1.

5.6 A SIMPLE SIMULATION CASE

Initial testing of the instruments revealed that sampling scopes are good at RJ and PJ decomposition, and real-time scopes are good at DCD and ISI separation. A simple simulation was run with the tool by simulating both a Bertscope pattern generator used as a transmitter and scopes from Tektronix. The simulation used a PRBS-9 signal running at 5Gbps. The rise time was found to be 21.7ps, and the fall time was 22.9ps, both at 20%-80% definition. The intrinsic RJ was 1.10ps. Using the jitter injection provision in the instrument, PJ of 2.05ps was injected at 4MHz. A voltage offset corresponding to DCD of 6ps was also added. A 9” trace was connected between the pattern generator and the two scopes, using low-loss cables. The waveform coming from the pattern generator had some distortion, which was simulated using a very small trace.

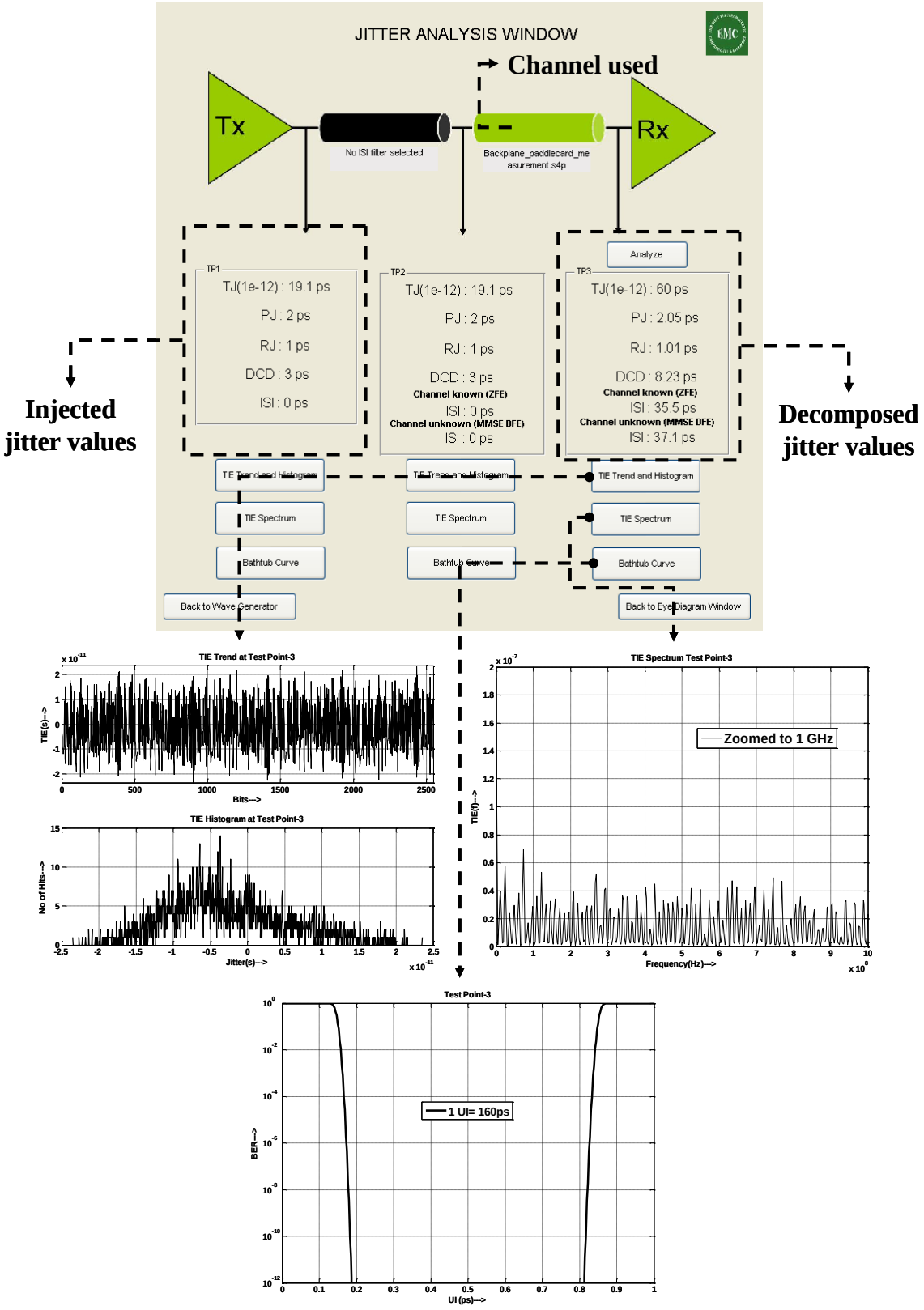

Figure 5.14. Jitter analysis GUI

Four single-ended S-parameter measurements were taken using PNA, the loaded in the tool; a) the distortion in the pattern generator waveform, b) cables, c) 9” trace and d) another cable. The single-ended waveform was distorted with the original jitter values, and the appropriate rise/fall time values were chosen to emulate the pattern generator. Figure 5.15 shows the cascaded S-parameter used in the simulation.

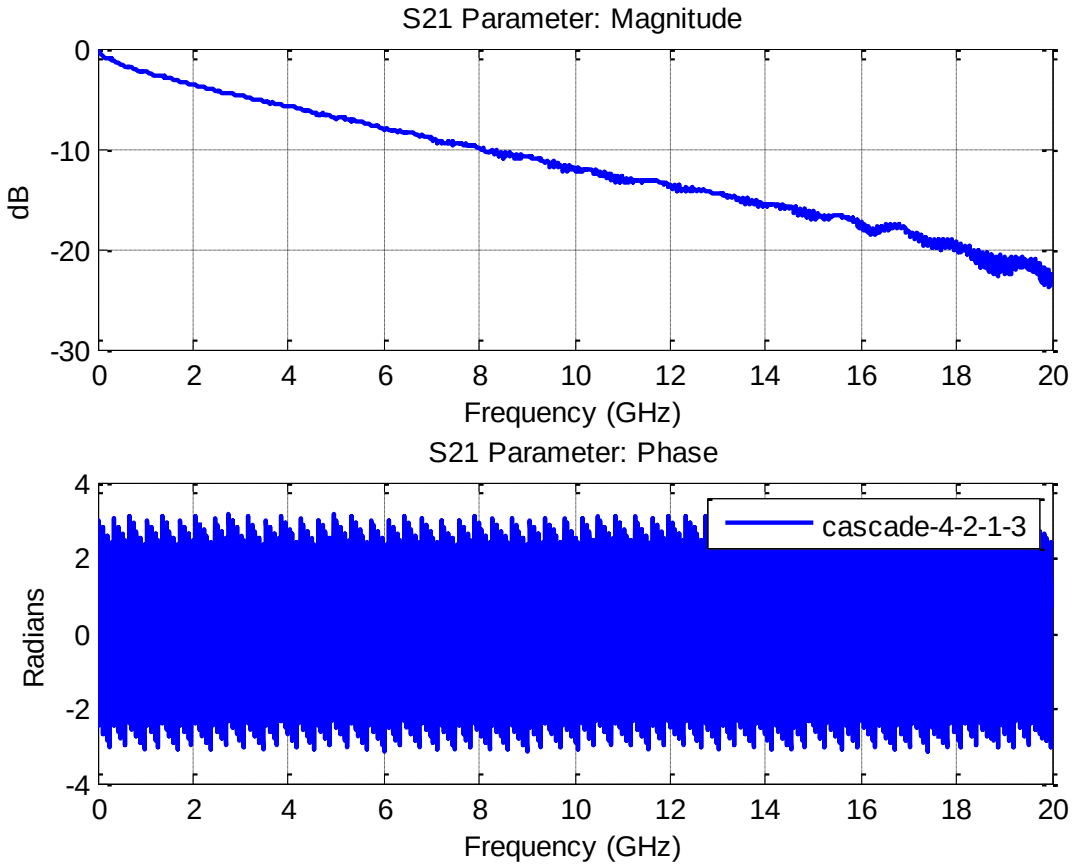

Figure 5.15. Cascaded S-Parameter used in the simulation

Figure 5.16 shows the laboratory setup used to take measurements in the lab and the injected values. A real-time scope was used to decompose DCD and ISI, and the sampling scope was used to separate PJ and RJ.

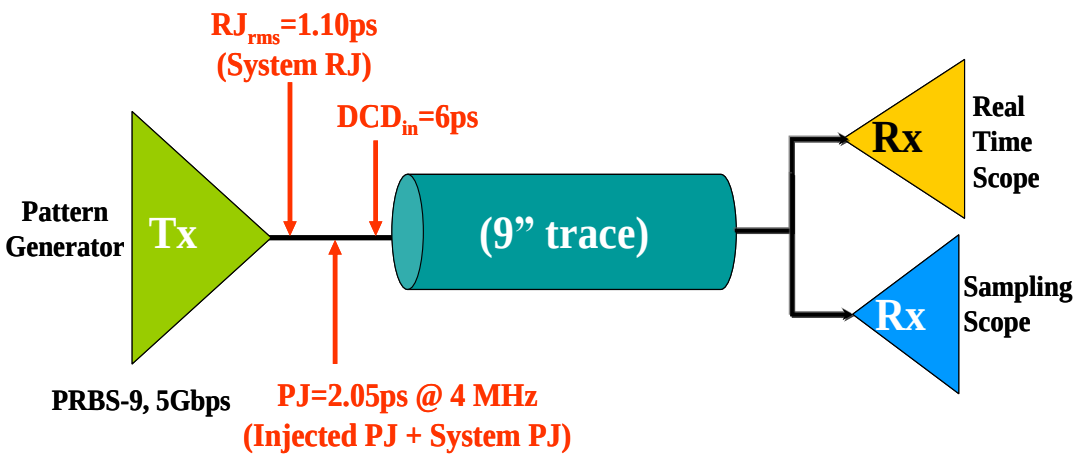

Figure 5.16. Measurement setup with the injected jitter values

Table 5.1 compares the decomposed jitter values from the instruments and the link path tool. The results show good correlation.

Table 5.1. Comparison of jitter decomposition results between instruments and tool

Jitter type / Results	PJ	RJ	DCD	ISI
Lab Results	1.97ps	1.09ps	12.01ps	14.25ps
Tool Results	1.97ps	1.04ps	12.67ps	15.16ps

The Bertscope pattern waveform had to modeled before the simulation was run. Several correlations were run with backplane channels, and the tool showed good correlation for the PJ and RJ decomposition. Problems arose, however, with the DCD and ISI separation, although they followed the same decomposition trend ISI was found to change with DCD injection, perhaps due to incorrect modeling of the pattern generator used. Figure 5.17 compares the bathtub curves at both channel ends.

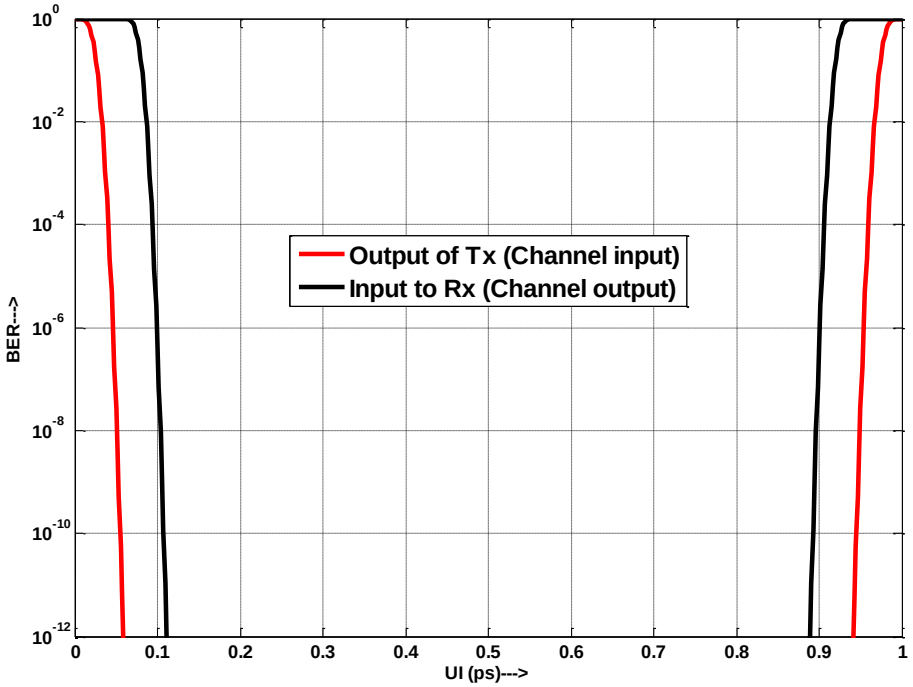

Figure 5.17. Bathtub curve comparison

5.7 CONCLUSIONS AND FUTURE WORK

The jitter models and decomposition methods developed here were based on technical and application notes from various vendors. A comparison was made among real-time scopes and sampling scopes from Tektronix, LeCroy, Agilent, and Bertscopes. Real-time scopes were found to decompose ISI and DCD properly, but they were poor at decomposing RJ and PJ. A common fault of real-time scopes was their tendencyto yield elevated values of PJ, depending on the type of pattern used. The sampling scopes gave proper values of PJ and RJ, but they gave elevated values of ISI and DCD. A comparison of jitter values yielded by real-time scopes from various vendors with those provided by sampling scopes from various vendors revealed many discrepancies. As a result, the tool was not thoroughly validated with commercial instruments. The data-dependent jitters obtained from the scopes were found to be elevated, perhaps due to incorrect pattern launching or reflections within the instrument themselves.

Careful investigation of jitter values obtained from instruments revealed that PJ and RJ should not have changed when they passed through a channel since they were uncorrelated to the data. In addition, ISI was found to increase when DCD was injected. The tool produced similar results. A detailed comparison between the tool and instruments is needed.

Jitter transformation can be properly studied using the tool along with the comparison of TIE spectrum and bathtub curves. The tool is not error free and fails to give reasonable values in some situations because it does not use the traditional approach. This is especially true of ISI values.

ISI calculation using the MMSE-DFE approach is not accurate always and depends on the linearity of the channel used and other factors. More study is required in this area. The MMSE-DFE approach has been included in the tool to help the user understand how close it is to the ISI value obtained from the other method.

This work did not model bounded uncorrelated jitter (BUJ) or crosstalk; such modeled will be an important additions to the tool in the future. Manifestation of the BUJ in the jitter spectrum is not yet understood and must be studied to develop a decomposition method for it.

6. CABLE CERTIFICATION TOOL

Small form factor pluggable (SFP+) modules are hot-pluggable serial-to-serial data-agnostic optical transceivers. They provide 10 Gigabit Ethernet connectivity options for data centers, enterprise wiring closets, and service provider transport applications [11]. They can be used in conjunction with optic fibers and copper cables. Figure 6.1 shows the various configurations of SFP+.

Figure 6.1. SFP+ configurations

When used in tandem with optic fibers, they can support link lengths of 26m and 10km depending on whether they use grade multimode fibers or standard single mode fibers. Transmission length, however is curtailed to 10m when they are used with copper cables. Table 37 of SFF-8431 standards (Revision 4.1) specifies 17 parameters needed to certify the SFP+ copper cable assembly and the measurement procedure for these parameters. The five parameters that have been coded into the cable certification tool are:

- dWDP (difference in dispersion penalty of output and input waveform)
- VMA (voltage modulation amplitude)
- DDPWS (pulse width shrinkage)
- Qsq (signal-to-noise ratio)
- RN (relative noise)

These parameters are not included in the standards but will be used directly and indirectly to calculate the 17 parameters needed to certify the cable. The standards apply to a PRBS-9 signal running at 10.3125Gbps. The rise/fall time is fixed at 34ps. The tool generates a word report with the calculated values. The values are compared with specified values to determine whether each parameter is within limits. The tool is in the initial stages of development; therefore this section will address only the calculation of the above 5 parameters with the screenshots of the GUI.

6.1 PARAMETER CALCULATION

The parameters that are calculated presently in the tool are dWDP, VMA, Qsq, RN and DDPWS. The first four of the five parameters calculated by the tool require the use of the transmitted wave dispersion penalty (TWDP) code specified in Appendix G of the SFP+ standards. Since the measurement applies to copper cables, an identity channel for copper must be selected. The code uses a minimum mean square error decision feedback equalizer (MMSE-DFE) with 14 T/2 FFE taps and 5 T spaced DFE taps.

6.1.1. dWDP. TWDP is a parameter used to quantify the performance of a transmitter [12-13]. These days, TWDP is used to determine whether a channel fails. Channel responses provide different levels of attenuation for each of the various frequency components. The end result is that a high speed digital signal suffers dispersion that is quantified by TWDP. TWDP is closely related to ISI [14]. Two inputs are needed

to calculate TWDP: output distorted waveform coming from the channel and the ideal data pattern used to generate the input waveform. For the SFP+ cable assembly, TWDP values need to be calculated both for the input signal and the output signal. The difference between these two values (WDP_i, WDP_o) represents the dWDP value. Figure 6.2 shows the setup used to calculate the values. The TWDP value for the input signal is constant and can be represented by a fixed number or an S-parameter file measured from the module compliance board to the host compliance board. The TWDP value for the output signal varies and is represented by an S-parameter file measured from module compliance board 1 to module compliance board 2. The WDP values are obtained by loading the corresponding S-parameter files and waveforms and running the TWDP code.

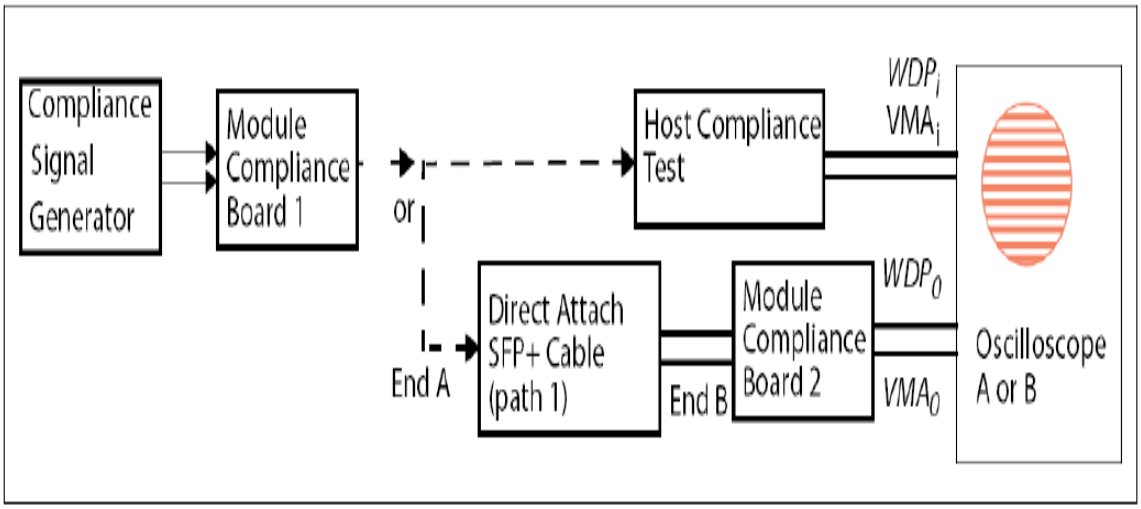

Figure 6.2. Measurement setup to obtain WDP_i, WDP_o, VMA_i and VMA_o

6.1.2. VMA, Qsq, and RN. VMA and Qsq are obtained directly from the TWDP code. RN is the inverse of Qsq.

6.1.3. DDPWS. DDPWS is a measure of the data-dependent jitter acquired by the signal after it passes through the channel. A simple calculation is used to measure the value.

$$DDPWS = T - \min(t_2 - t_1, t_3 - t_2, ... t_{n+1} - t_n) \quad (18)$$

Figure 6.3 compares a distorted waveform and its ideal counterpart which are used in making the calculation.

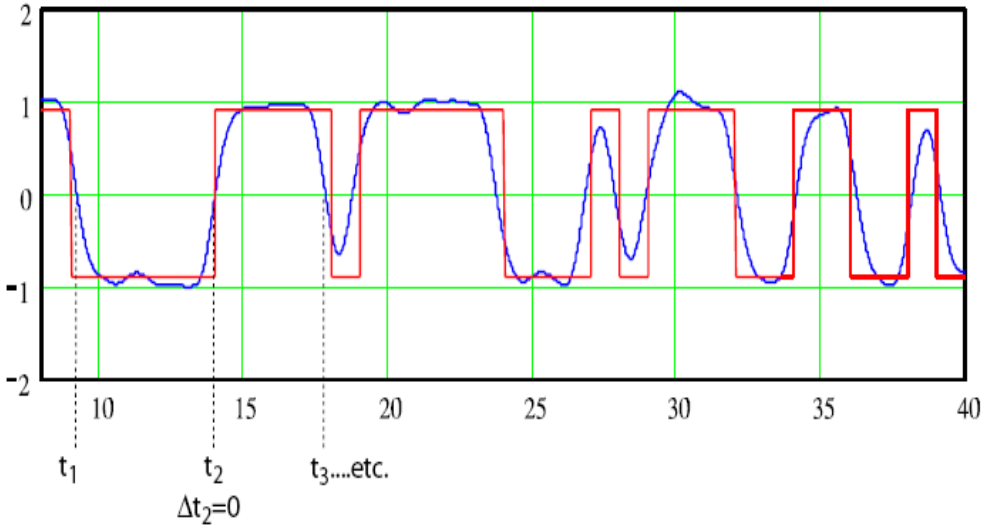

Figure 6.3. Comparison between distorted waveform and ideal counterpart

A code calculates the zero crossing points (t_1, t_2 …t_n). The second quantity in the above equation is calculated and is subtracted from the bit period (T), which is approximately 97ps (10.3125Gbps), to get the DDPWS value.

6.2 TOOL GUI

Figure 6.4 shows the initial tool GUI. When the user clicks on the Load S-Parameters button, another window opens displaying an option to load the S-parameter files.

Figure 6.4. Tool launch GUI

The S-parameter manager GUI allows the user to load the 4-port differential files measured from module compliance board-1 to module compliance board-2. These are touchstone files that are saved from VNA measurements used to measure WDP_o and VMA_o. The values of WDP_i and VMA_i are constant, and the measurement is performed in the background. This is the point at which the S-parameter values are preprocessed. Passivity and causality are checked and enforced if necessary. In most cases, the S-parameter data must be extrapolated to zero frequency and interpolated at a particular frequency sampling rate. This process ensures proper time domain data after an IFFT is taken. Provision to view the magnitude and phase plot is included in this portion. The user can change the port numbering if a different port configuration was selected VNA measurements. Figure 6.5 shows the S-parameter manager GUI with a loaded s4p file.

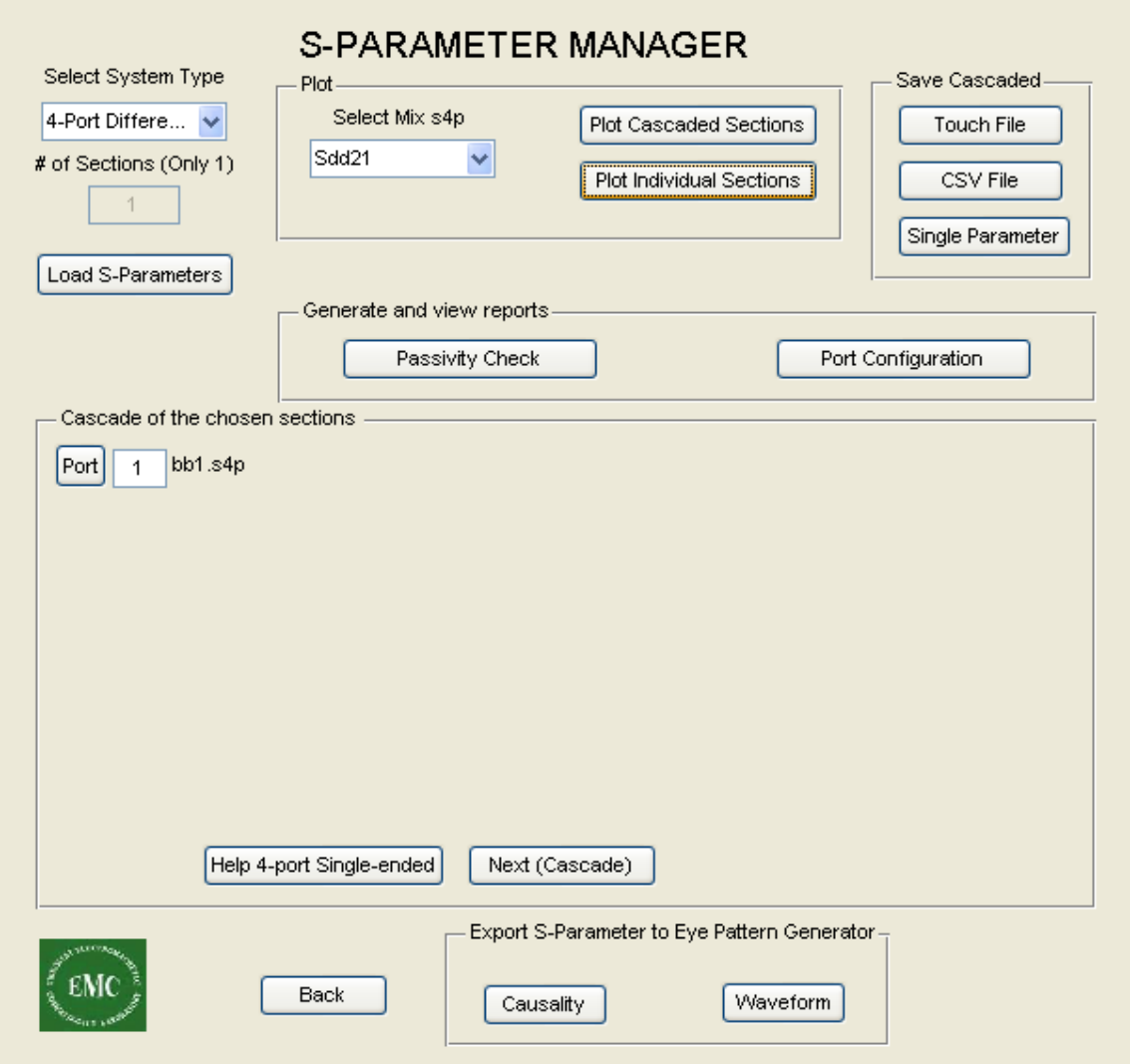

Figure 6.5. S-Parameter manager GUI

The next window defines the time-domain input waveform. The user has the option to select either a single-ended or differential-signal configuration. The parameters that can be defined here are bit-rate, number of samples per bit, type of pattern, rise/fall time, and voltage amplitude. The user may wish to add additional jitter and emphasis to the time-domain waveform. Once the waveform is generated, it is converted into frequency domain by taking a fourier transform. It is then multiplied with the S-parameter data to obtain the output-distorted waveform in the frequency domain. A time domain representation of this waveform can be obtained by taking an inverse fourier

transform on which all the necessary SFP+ calculations have been performed. The calculations require the data pattern originally used to create the input waveform. Figure 6.6 displays the waveform generator GUI.

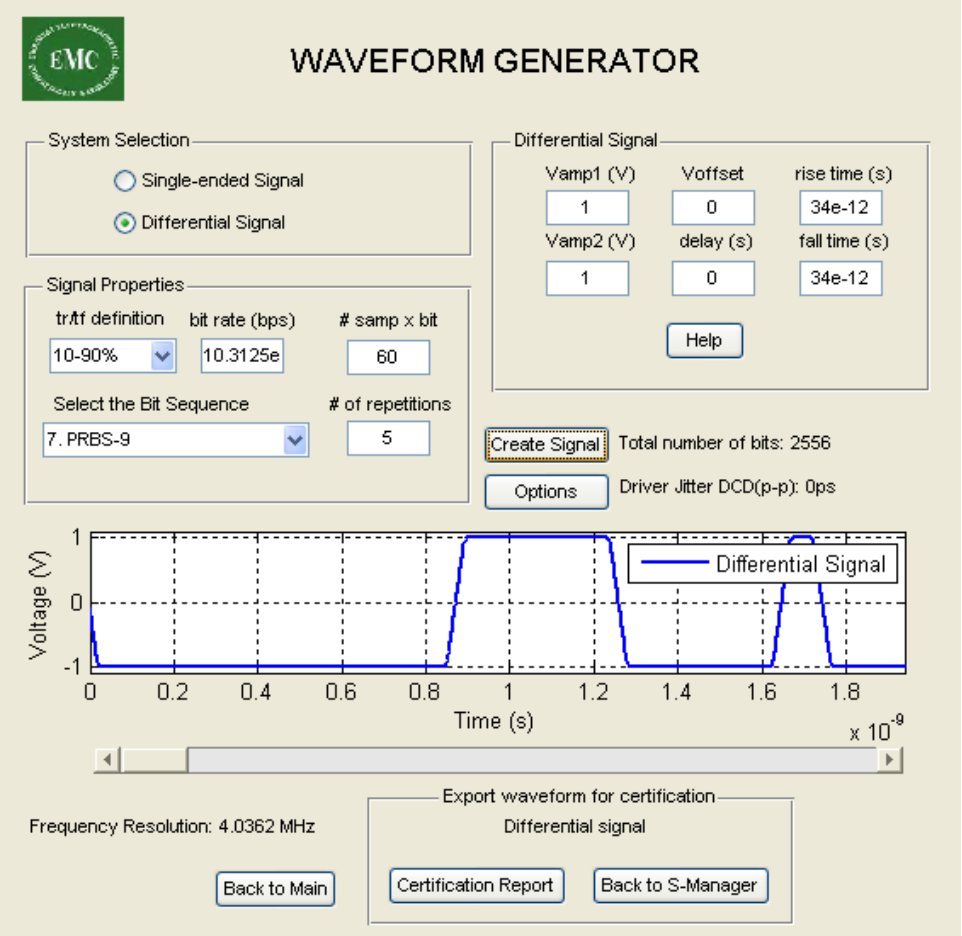

Figure 6.6. Waveform generator GUI

Once the user clicks on the certification report on the waveform generator, another GUI opens on which the various parameters are calculated. As noted above, the TWDP calculation requires inputs of both the distorted waveform and the ideal data pattern used to construct the waveform. The same TWDP code measures VMA, Qsq, and RN. The DDPWS is calculated by running another code that obtains the crossing points

of each transition in the waveform and using the corresponding equation. Figure 6.7 shows the corresponding GUI with the calculated values. The user may wish to generate the results in a Word file report which displays the calculated values and compares the input and output waveform and the eye-diagram.

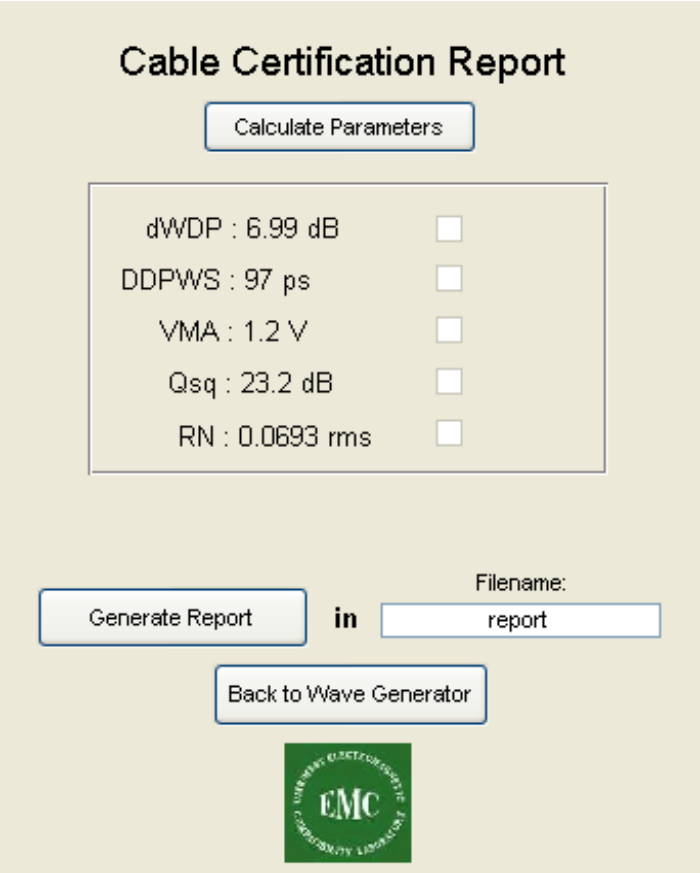

Figure 6.7. Cable certification report GUI

6.3 CONCLUSIONS AND FUTURE WORK

The tool calculates the SFP+ parameters without the need for expensive instruments. The only input from the industry side is the touchstone S-parameter files, which must be obtained through a VNA measurement. Ideally, the compliance generator used in setup should be an ideal generator with no intrinsic RJ and PJ. The tool can

emulate the nonideal compliance generator by injecting jitter. The tool calculates five parameters that directly and indirectly help to calculate the required 17 parameters needed to certify the cable. Figure 6.8 shows the arrangement of the report generated in Word.

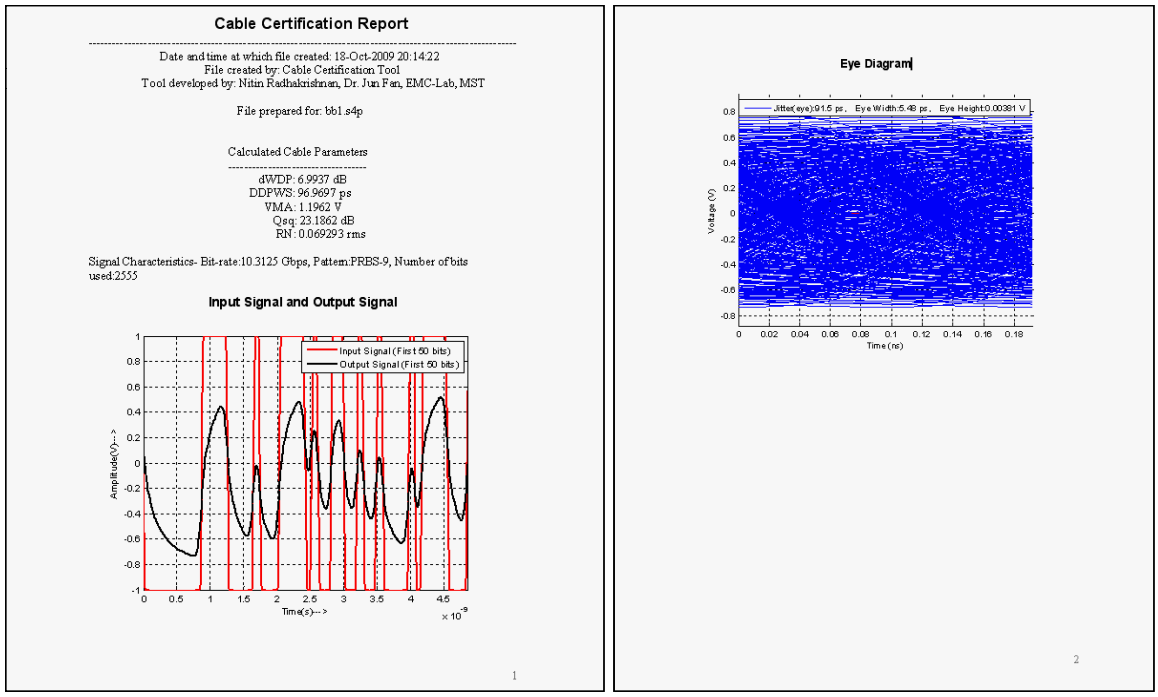

Figure 6.8. Word report

There are two differential pairs in one cable. One represents the transmitter (Tx) and other the receiver (Rx). For each differential pair, eight parameters are specified. If WDP_i is included, a total of 17 parameters should be calculated for a single cable. Future work will redesign the GUI to calculate these parameters. All 17 parameters must be compared with the specified values. Based on this comparison, the cable can be certified as pass or fail. Future work will modify the report to accommodate these changes.

In addition, the tool must be modified/enhanced so that configuration files can be saved. The user should be able to load the file in the GUI or run the program with

different file settings. Finally, actual measurements must be made on SFP+ cable to validate the results.

BIBLIOGRAPHY

[1] Mike Peng Li, "Jitter, Noise and Signal Integrity at High-Speed," 1st ed., Prentice Hall, 2007.

[2] Application note, "Understanding Jitter," Wavecrest Corporation, 2001.

[3] Clayton R. Paul, "Introduction to Electromagnetic Compatibility," 2nd ed., Wiley-Interscience, 2006.

[4] SFF-8431 Specifications for Enhanced 8.5 and 10 Gigabit Small Form Factor Pluggable Module SFP+, Revision 4.1, 6 July 2009.

[5] Kyung Ki Kim, Jing Huang, Yong-Bin Kim, Fabrizio Lombardi, "Analysis and Simulation of Jitter Sequences for Testing Serial Data Channels," IEEE Transactions on Industrial Informatics, Vol.4, No.2, May 2008.

[6] Application note, "Understanding and Characterizing Timing Jitter," Tektronix, 2003.

[7] Application note, "Analyzing Jitter Using a Spectrum Approach," Tektronix 2002.

[8] Application note, "Bertscope Jitter Map 'Under the Hood'-A New Methodology for Jitter Separation," SyntheSys Research Inc., 2009.

[9] White paper, "Jitter Analysis: The dual-Dirac Model, RJ/PJ, and Q-Scale," Agilent Technologies, 2005.

[10] White paper, "Equalization: The Correction and Analysis of Degraded Signals," Agilent Technologies, 2005.

[11] Data Sheet, Cisco 10GBASE SFP+ Module, 2008.

[12] IEEE Std 802.3aq, 2006.

[13] Norman L. Swenson, Paul Voois, Tom Lindsay, Steve Zeng, "Standards compliance testing of optical transmitters using a software-based equalizing reference receiver."

[14] Surbhi Mittal, Francesco De Paulis, Zhiping Yang, Jun Fan, "Using TWDP to Quantify Channel Performance with Frequency-Domain S-Parameter Data."

VITA

Nitin Radhakrishnan was born on January 14th, 1983 in Benghazi, Libya. In May 2005, he obtained his Bachelor's degree in Electronics and Telecommunications from SCT College of Engineering, Trivandrum, India.

In January 2006, he enrolled at the Missouri University of Science and Technology to pursue his Master's Degree in Electrical Engineering and received his first Master's Degree in December 2007.

In January 2008, he enrolled in the same university for another Master's Degree in Computer Engineering during which time he was a graduate research assistant in Electromagnetic Compatibility Laboratory. From January 2009 to August 2009, he did an internship at Cisco Systems., San Jose, California. He received his second Master's Degree in December 2009.